TeV scale modified type-II seesaw mechanism and dark matter in a gauged $U(1)_{B-L}$ symmetric model

Purusottam Ghosh,[1,*] Satyabrata Mahapatra,[2,†] Nimmala Narendra,[3,‡] and Narendra Sahu[2,§]

[1]*Regional Centre for Accelerator-based Particle Physics, Harish-Chandra Research Institute, HBNI, Chhatnag Road, Jhunsi, Allahabad—211 019, India*

[2]*Department of Physics, Indian Institute of Technology Hyderabad, Kandi, Sangareddy 502285, Telangana, India*

[3]*Theoretical Physics Division, Physical Research Laboratory, Ahmedabad 380009, India*

(Received 13 January 2022; accepted 16 June 2022; published 5 July 2022)

In an endeavor to explain the light neutrino masses and dark matter (DM) simultaneously, we study a gauged $U(1)_{B-L}$ extension of the standard model (SM). The neutrino masses are generated through a variant of type-II seesaw mechanism in which one of the scalar triplets has a mass in a scale that is accessible at the present generation colliders. Three SM singlet right chiral fermions χ_{iR} $(i = e, \mu, \tau)$ with $B - L$ charges -4, -4, $+5$ are invoked to cancel the $B - L$ gauge anomalies and the lightest one among these three fermions becomes a viable DM candidate as their stability is guaranteed by a remnant $\mathcal{Z}_2$ symmetry to which $U(1)_{B-L}$ gauge symmetry gets spontaneously broken. Interestingly in this scenario, the neutrino mass and the coannihilation of DM are interlinked through the breaking of $U(1)_{B-L}$ symmetry. Apart from giving rise to the observed neutrino mass and dark matter abundance, the model also predicts exciting signals at the colliders. Especially we see a significant enhancement in the production cross section of the TeV scale doubly charged scalar in presence of the Z_{BL} gauge boson. We discuss all the relevant constraints on model parameters from observed DM abundance and null detection of DM at direct and indirect search experiments as well as the constraints on the $B - L$ gauge boson from recent colliders.

DOI: 10.1103/PhysRevD.106.015001

I. INTRODUCTION

Out of all the lacunae afflicting the Standard Model (SM) of particle physics, the identity of DM and the origin of tiny but nonzero neutrino masses are the most irking ones. It is well established by now, thanks to numerous irrefutable observational evidences from astrophysics and cosmology like galaxy rotation curves, gravitational lensing, Cosmic Microwave Background (CMB) acoustic oscillations etc., [1–6], that a mysterious, nonluminous and nonbaryonic form of matter exists called as dark matter (DM) which constitutes almost 85% of the total matter content and around 26.8% of the total energy density of the present Universe. In terms of density parameter $h = (\text{Hubble Parameter})/(100\ \text{km s}^{-1}\ \text{Mpc}^{-1})$, the present DM abundance is conventionally reported as [5,6]: $\Omega_{DM}h^2 = 0.120 \pm 0.001$. But still we have no answer to the question what DM actually is, as none of the SM particle has the properties that a DM particle is expected to have. Thus over the years, various beyond SM (BSM) scenarios have been considered to explain the puzzle of DM, with additional field content and augmented symmetry. The most popular among these ideas is something known as the weakly interacting massive particle (WIMP) paradigm. In this WIMP scenario, a DM candidate typically having a mass similar to electroweak (EW) scale and interaction rate analogous to EW interactions can give rise to the correct DM relic abundance, an astounding coincidence referred to as the *WIMP miracle* [7,8]. The sizeable interactions of WIMP DM with the SM particles has many phenomenological implications. Along with giving the correct relic abundance of DM through thermal freeze-out, it also leads to other phenomenological implications like optimistic direct and indirect detection prospects of DM which makes it more appealing. Several direct detection experiments like LUX, PandaX-II, and XENON1T [9–13] and indirect detection experiments like space-based telescopes Fermi-LAT and ground-based telescopes MAGIC [14,15] have been looking for signals of DM and have put constraints on DM-nucleon scattering cross

*purusottamghosh@hri.res.in
†ph18resch11001@iith.ac.in
‡nnarendra@prl.res.in
§nsahu@phy.iith.ac.in

sections and DM annihilation cross section to SM particles respectively.

Apart from the identity of DM, another appealing motivation for the BSM is the origin of neutrino masses. Despite compelling evidences for existence of light neutrino masses, from various oscillation experiments [16–20] and cosmological data [21–24], the origin of light neutrino masses is still unknown. The oscillation data is only sensitive to the difference in mass-squareds [21,25], but the absolute mass scale is constrained to $\sum_i |m(\nu_i)| < 0.12$ eV [21] from cosmological data. This also implies that we need new physics in BSM to incorporate the light neutrino masses as the Higgs field, which lies at the origin of all massive particles in the SM, cannot have any Yukawa coupling with the neutrinos due to the absence of its right-handed counterpart.

Assuming that the neutrinos to be of Majorana type (which violates lepton number by two units), the origin of the tiny but nonzero neutrino mass is usually explained by the seesaw mechanisms (type-I [26–30], type-II [31–35] and type-III [36]) which are the ultraviolet completed realizations of the dimension five Weinberg operator $\mathcal{O}_5 = y_{ij}\frac{\overline{L_i}L_j^c HH}{\Lambda}$, where L and H are the lepton and Higgs doublets of the SM and Λ is the scale of new physics [37,38]. In the type-I seesaw heavy singlet RHNs are introduced while in type-II and type-III case, a triplet scalar(Δ) of hypercharge 2 and triplet fermions Σ of hypercharge 0 are introduced respectively such that new Yukawa terms can be incorporated in the theory. Tuning the Yukawa coupling and the cutoff scale (Λ) and adopting a necessary structure for the mass matrix, the correct masses and mixings of the neutrinos can be obtained.

In the conventional type-II seesaw, the relevant terms in the Lagrangian violating lepton number by two units are $f_{ij}\Delta L_i L_j + \mu\Delta^\dagger HH$, where Δ does not acquire an explicit vacuum expectation value (vev). However, after the electroweak phase transition, a small induced vev of Δ can be obtained as: $\langle\Delta\rangle = -\frac{\mu\langle H\rangle^2}{M_\Delta^2}$. Thus for $\mu \sim M_\Delta \sim 10^{14}$ GeV, one can get $M_\nu = f\langle\Delta\rangle \simeq f\frac{\langle H\rangle^2}{M_\Delta}$ of order $\mathcal{O}(0.1)$ eV for $f \sim 1$.

In an alternative fashion, neutrino mass can be generated in a modified type-II seesaw if one introduces two scalar triplets: Δ and ξ with $M_\Delta \sim \mathcal{O}(10^3)$ TeV and $M_\xi \sim$ TeV $\ll M_\Delta$ [39].[1] In this case imposition of additional B − L gauge symmetry [41] allows for $\mu\Delta^\dagger HH + f\xi LL + y\Phi_{\rm BL}^2\Delta^\dagger\xi$ terms in the Lagrangian (with proper choice of gauge charges for the scalars) where $\Phi_{\rm BL}$ is the scalar field responsible for B − L symmetry breaking at TeV scale. As is clear from the Lagrangian terms, once the $\Phi_{\rm BL}$ acquires a vev, it creates a small mixing between Δ and ξ of the order $\theta \sim \frac{\langle\Phi_{\rm BL}\rangle^2}{M_\Delta^2} \simeq 10^{-6}$. Thus the coupling of ξ with Higgs becomes extremely suppressed but ξLL coupling can be large. In this scenario, Δ being super heavy gets decoupled from the low energy effective theory but ξ can have mass from several hundred GeV to a few TeV and having large dilepton coupling can be probed at colliders through the same sign dilepton signature [42–48].

In this paper, we implement such a modified type-II seesaw in a gauged $U(1)_{\rm B-L}$ symmetric model and study the consequences for dark matter, neutrino mass and collider signatures. We introduce three right chiral fermions χ_{i_R} $(i = e,\ \mu,\ \tau)$ with $U(1)_{\rm B-L}$ charges $-4, -4, +5$ for cancellation of nontrivial gauge and gravitational anomalies. For the details of the anomaly cancellation in a B − L model, please see Appendix A. Interestingly, the lightest one among these three exotic fermions becomes a viable candidate of DM, thanks to the remnant $\mathcal{Z}_2$ symmetry after $U(1)_{\rm B-L}$ breaking, under which χ_{i_R} $(i = e,\ \mu,\ \tau)$ are odd while all other particles are even.[2] Such an alternative integral B − L charge assignment solution for the additional fermions to achieve anomaly cancellation was first proposed in [51] and its phenomenology have been studied in different contexts relating to fermionic DM and neutrino mass in [52–56].[3] In these earlier studies, the relic abundance of DM is usually determined by the annihilation cross section through the freeze-out mechanism, which results in satisfying the correct relic density near the resonances. Here we study the effect of both annihilation and coannihilations among the dark sector particles in the presence of additional scalar and its implication on the viable parameter space consistent with all phenomenological and experimental constraints.

The origin of neutrino mass and DM is hitherto not known. Any connection between them is also not established yet. However, it will really be interesting if neutrino mass and the DM phenomenology have an interconnection between them. In light of this, it is worth mentioning here that the spontaneous breaking of $U(1)_{\rm B-L}$ gauge symmetry via the vev of $\Phi_{\rm BL}$ not only generates sub-eV masses of light neutrinos, but also gives rise to coannihilations among the dark sector fermions in this study.

The doubly charged scalar in this model offers novel multi-lepton signatures with missing energy and jets which has already been studied in the literature [42–48]. However, as this doubly charged scalar possesses both SM gauge

[1]See also Ref. [40] for a modified double type-II seesaw with TeV scale scalar triplet.

[2]Right-handed neutrinos with B − L charge −1 can also serve the purpose of B − L anomaly cancellation and be viable DM candidate provided one introduces an additional *ad hoc* $\mathcal{Z}_2$ symmetry to guarantee their stability. For instance see [49,50].

[3]In an earlier preliminary project [57], we had studied this model with the same motivation. The present work is an extended version with a detailed study of coannihilation effect and additional focus on collider signature of doubly charged scalars in a gauged B − L scenarios.

charges as well as B − L gauge charge in this scenario, we study the effect of the B − L gauge boson on the production probability of such a doubly charged scalar. In particular, for a TeV scale doubly charged scalar, we show that the production cross section can get enhanced significantly if the presence of B − L gauge boson which has mass in a few TeV range.

The rest of the paper is organized as follows. In Sec. II, we describe the proposed model, the neutrino mass generation through a variant of type-II seesaw, the scalar masses and mixing. We then discuss how the particles introduced for anomaly cancellation become viable DM candidate and study the relic density in Sec. III. In Sec. IV, we studied all the relevant constraints from direct, indirect search of DM on our parameter space as well as scrutinized it with respect to the constraint from colliders. We briefly summarize the collider search strategies of the model in Sec. V and finally conclude in Sec. VI.

II. THE MODEL

The model under consideration is a very well motivated BSM framework based on the gauged $U(1)_{\mathrm{B-L}}$ symmetry [58–63] in which we implement a modified type-II seesaw to explain the sub-eV neutrino mass by introducing two triplet scalars Δ and ξ. Δ is super heavy with $M_\Delta \sim 10^3$ TeV and $M_\xi \sim$ TeV $\ll M_\Delta$ and the B − L charges of Δ and ξ are 0 and 2 respectively. As already discussed in the previous section, the additional $U(1)_{\mathrm{B-L}}$ gauge symmetry introduces B − L anomalies in the theory. To cancel these B − L anomalies we introduce three right chiral dark sector fermions χ_{i_R} $(i = e,\ \mu,\ \tau)$, where the B − L charges of $\chi_{e_R}\chi_{\mu_R}$ and χ_{τ_R} are −4, −4, +5 respectively. Note that such unconventional B − L charge assignment of the $\chi_{i_R}(i = e,\mu,\tau)$ forbids their Yukawa couplings with the SM particles. Also three singlet scalars: Φ_{BL}, Φ_{12}, and Φ_3 with B − L charges −1, +8, −10 are introduced. As a result of which Φ_{12} and Φ_3 couple to χ_{e_R,μ_R} and χ_{τ_R} respectively through Yukawa terms and the vevs of Φ_{12} and Φ_3 provides Majorana masses to these dark sector fermions. The vev of Φ_{BL} provides a small mixing between Δ and ξ which plays a crucial role in generating sub-eV masses of neutrinos. This vev $\langle\Phi_{\mathrm{BL}}\rangle$ is also instrumental in controlling the coannihilations among the dark sector particles and hence is crucial for DM phenomenology too. As a consequence this establishes an interesting correlation between the neutrino mass and DM. The particle content and their charge assignments are listed in Table I.

The Lagrangian involving the BSM fields consistent with the extended symmetry is given by:

$$\mathcal{L} = \mathcal{L}^{\mathrm{SM+BSM\ Scalar}} + \mathcal{L}^{\mathrm{DM}}, \tag{1}$$

where

$$\begin{aligned}\mathcal{L}^{\mathrm{SM+BSM\ Scalar}} \supset\ & |D_\mu H|^2 + |D_\mu \Phi_3|^2 + |D_\mu \Phi_{\mathrm{BL}}|^2 + |D_\mu \Phi_{12}|^2 \\ & + \mathrm{Tr}[(D_\mu \Delta)^\dagger (D^\mu \Delta)] + \mathrm{Tr}[(D_\mu \xi)^\dagger (D^\mu \xi)] \\ & - Y^{\xi}_{ij} \overline{L^c_i} i\tau_2 \xi L_j - \mathrm{V}^{\mathbb{L}}(H,\xi,\Phi_3) \\ & - V^{\mathbb{H}}(\Delta,\Phi_{\mathrm{BL}},\Phi_{12}) - V^{\mathbb{LH}}. \end{aligned} \tag{2}$$

Here i, j runs over all three lepton generations. In the above Lagrangian, $\mathrm{V}^{\mathbb{L}}$ is the scalar potential involving scalars in sub-TeV mass range (H,ξ,Φ_3), $\mathrm{V}^{\mathbb{H}}$ stands for scalar potential of the heavy fields $(\Delta,\Phi_{\mathrm{BL}},\Phi_{12})$ and the scalar potential which involves both sub-TeV and super heavy fields is defined by $\mathrm{V}^{\mathbb{LH}}$.

The covariant derivatives for these fields can be written as:

$$\begin{aligned} D_\mu H &= \partial_\mu H + igT^a W^a_\mu H + ig' B_\mu H \\ D_\mu \Delta &= \partial_\mu \Delta + ig[T^a W^a_\mu, \Delta] + ig' Y B_\mu \Delta \\ D_\mu \xi &= \partial_\mu \xi + ig[T^a W^a_\mu, \xi] + ig' Y B_\mu \xi + ig_{\mathrm{BL}} Y_{\mathrm{BL}} (Z_{\mathrm{BL}})_\mu \xi \\ D_\mu G &= \partial_\mu G + ig_{\mathrm{BL}} Y_{\mathrm{BL}} (Z_{\mathrm{BL}})_\mu G \\ &\quad \text{where } G = \{\Phi_3, \Phi_{\mathrm{BL}}, \Phi_{12}\}. \end{aligned}$$

TABLE I. Charge assignment of BSM fields under the gauge group $\mathcal{G} \equiv \mathcal{G}_{\mathrm{SM}} \otimes U(1)_{B-L}$, where $\mathcal{G}_{\mathrm{SM}} \equiv SU(3)_C \otimes SU(2)_L \otimes U(1)_Y$.

BSM fields		$SU(3)_C \otimes SU(2)_L \otimes U(1)_Y$			$\otimes\ U(1)_{\mathrm{B-L}}$
Dark sector fermions	χ_{e_R}, χ_{μ_R}	1	1	0	−4
	χ_{τ_R}	1	1	0	5
Heavy scalars	$\Delta = \begin{pmatrix} \frac{\delta^+}{\sqrt{2}} & \delta^{++} \\ \delta^0 & -\frac{\delta^+}{\sqrt{2}} \end{pmatrix}$	1	3	2	0
	Φ_{BL}	1	1	0	−1
	Φ_{12}	1	1	0	8
Light scalars	$\xi = \begin{pmatrix} \frac{\xi^+}{\sqrt{2}} & \xi^{++} \\ \xi^0 & -\frac{\xi^+}{\sqrt{2}} \end{pmatrix}$	1	3	2	2
	Φ_3	1	1	0	−10

The Lagrangian of the dark sector can be written as:

$$\begin{aligned}\mathcal{L}^{\rm DM} &= \overline{\chi_{e_R}} i\gamma^\mu D_\mu \chi_{e_R} + \overline{\chi_{\mu_R}} i\gamma^\mu D_\mu \chi_{\mu_R} + \overline{\chi_{\tau_R}} i\gamma^\mu D_\mu \chi_{\tau_R} \\ &+ Y_{11}\Phi_{12}\overline{(\chi_{e_R})^c}\chi_{e_R} + Y_{22}\Phi_{12}\overline{(\chi_{\mu_R})^c}\chi_{\mu_R} \\ &+ Y_{12}\Phi_{12}\overline{(\chi_{e_R})^c}\chi_{\mu_R} + Y_{13}\Phi_{\rm BL}\overline{(\chi_{e_R})^c}\chi_{\tau_R} \\ &+ Y_{23}\Phi_{\rm BL}\overline{(\chi_{\mu_R})^c}\chi_{\tau_R} + Y_{33}\Phi_3\overline{(\chi_{\tau_R})^c}\chi_{\tau_R} + \text{H.c.}, \quad (3)\end{aligned}$$

where

$$D_\mu\chi = \partial_\mu\chi + i g_{\rm BL} Y_{\rm BL} (Z_{\rm BL})_\mu \chi.$$

The gauge coupling associated with $U(1)_{\rm B-L}$ is $g_{\rm BL}$ and $Z_{\rm BL}$ is the corresponding gauge boson. The scalar potentials which are mentioned in the Lagrangian (2) can be written as:

$$\begin{aligned}\mathrm{V}^{\mathbb{L}}(H,\xi,\Phi_3) &= -\mu_H^2 H^\dagger H + \lambda_H (H^\dagger H)^2 + M_\xi^2 \mathrm{Tr}[\xi^\dagger\xi] + \lambda_\xi (\mathrm{Tr}[\xi^\dagger\xi])^2 + \lambda'_\xi \mathrm{Tr}[(\xi^\dagger\xi)^2] + \lambda_{\xi H}\mathrm{Tr}[\xi^\dagger\xi](H^\dagger H) + \lambda'_{\xi H}(H^\dagger\xi\xi^\dagger H) \\ &- \mu_{\Phi_3}^2 \Phi_3^\dagger\Phi_3 + \lambda_{\Phi_3}(\Phi_3^\dagger\Phi_3)^2 + \lambda_{H\Phi_3}(H^\dagger H)(\Phi_3^\dagger\Phi_3) + \lambda_{\xi\Phi_3}(\Phi_3^\dagger\Phi_3)\mathrm{Tr}[\xi^\dagger\xi], \quad (4)\end{aligned}$$

$$\begin{aligned}\mathrm{V}^{\mathbb{H}}(\Delta,\Phi_{\rm BL},\Phi_{12}) &= M_\Delta^2 \mathrm{Tr}[\Delta^\dagger\Delta] + \lambda_\Delta(\mathrm{Tr}[\Delta^\dagger\Delta])^2 + \lambda'_\Delta \mathrm{Tr}[(\Delta^\dagger\Delta)^2] - \mu_{\Phi_{\rm BL}}^2 \Phi_{\rm BL}^\dagger\Phi_{\rm BL} + \lambda_{\Phi_{\rm BL}}(\Phi_{\rm BL}^\dagger\Phi_{\rm BL})^2 \\ &+ \lambda_{\Delta\Phi_{\rm BL}}\mathrm{Tr}[\Delta^\dagger\Delta](\Phi_{\rm BL}^\dagger\Phi_{\rm BL}) - \mu_{\Phi_{12}}^2\Phi_{12}^\dagger\Phi_{12} + \lambda_{\Phi_{12}}(\Phi_{12}^\dagger\Phi_{12})^2 + \lambda_{\Delta\Phi_{12}}\mathrm{Tr}[\Delta^\dagger\Delta](\Phi_{12}{}^\dagger\Phi_{12}) \\ &+ \lambda_{\Phi_{\rm BL}\Phi_{12}}(\Phi_{\rm BL}^\dagger\Phi_{\rm BL})(\Phi_{12}{}^\dagger\Phi_{12}) + \lambda'_{\Phi_{\rm BL}\Phi_{12}}(\Phi_{\rm BL}^\dagger\Phi_{12})(\Phi_{12}{}^\dagger\Phi_{\rm BL}), \quad (5)\end{aligned}$$

$$\begin{aligned}\mathrm{V}^{\mathbb{LH}} &= \lambda_{\Delta H}\mathrm{Tr}[\Delta^\dagger\Delta](H^\dagger H) + \lambda'_{\Delta H}(H^\dagger\Delta\Delta^\dagger H) + [\mu_\Delta(H^T i\sigma^2\Delta^\dagger H) + H.c] \\ &+ \lambda_{H\Phi_{\rm BL}}(H^\dagger H)(\Phi_{\rm BL}^\dagger\Phi_{\rm BL}) + \lambda_{H\Phi_{12}}(H^\dagger H)(\Phi_{12}{}^\dagger\Phi_{12}) + \lambda_{\Phi_{\rm BL}\Phi_3}(\Phi_{\rm BL}^\dagger\Phi_{\rm BL})(\Phi_3^\dagger\Phi_3) \\ &+ \lambda'_{\Phi_{\rm BL}\Phi_3}(\Phi_{\rm BL}^\dagger\Phi_3)(\Phi_3^\dagger\Phi_{\rm BL}) + \lambda_{\Phi_{12}\Phi_3}(\Phi_{12}{}^\dagger\Phi_{12})(\Phi_3^\dagger\Phi_3) + \lambda'_{\Phi_{12}\Phi_3}(\Phi_{12}{}^\dagger\Phi_3)(\Phi_3^\dagger\Phi_{12}) \\ &+ \lambda_{\Delta\Phi_3}(\Delta^\dagger\Delta)(\Phi_3^\dagger\Phi_3) + \lambda_{\xi\Phi_{\rm BL}}\mathrm{Tr}[\xi^\dagger\xi](\Phi_{\rm BL}^\dagger\Phi_{\rm BL}) + \lambda_{\xi\Phi_{12}}\mathrm{Tr}[\xi^\dagger\xi](\Phi_{12}{}^\dagger\Phi_{12}) \\ &+ \lambda_{\Delta\xi}\mathrm{Tr}[\Delta^\dagger\Delta]\mathrm{Tr}[\xi^\dagger\xi] + \lambda'_{\Delta\xi}\mathrm{Tr}[\Delta^\dagger\xi]\mathrm{Tr}[\xi^\dagger\Delta] + \lambda_P\Phi_{\rm BL}^2\mathrm{Tr}[\Delta^\dagger\xi] + \lambda_Q(\Phi_{\rm BL}^\dagger)^2\Phi_3\Phi_{12} + \text{H.c.} \quad (6)\end{aligned}$$

Here it is worth mentioning that the mass squared terms of Δ and ξ are chosen to be positive so they do not get any spontaneous vev. Only the neutral components of H, Φ_{12}, $\Phi_{\rm BL}$, and Φ_3 acquire nonzero vevs. However, after electroweak phase transition, Δ and ξ acquire induced vevs.

For simplicity, we assume a certain mass hierarchy among the scalars. The masses of H, Φ_3 and ξ are of similar order in sub-TeV range, while the masses of $\Phi_{\rm BL}$ and Φ_{12} are in the several TeV scale. To make the analysis simpler, we decouple the light scalar sector from the heavy scalar sector by considering all quartic couplings in the scalar potential $\mathrm{V}^{\mathbb{LH}}$ to be negligible. It is worth mentioning that this assumption does not affect our DM phenomenology.

We parametrize the low energy neutral scalars as:

$$H^0 = \frac{v_H + h_H + iG_H}{\sqrt{2}}, \qquad \xi^0 = \frac{v_\xi + h_\xi + iG_\xi}{\sqrt{2}},$$
$$\Phi_3 = \frac{v_3 + h_3 + iG_{\Phi_3}}{\sqrt{2}}.$$

A. Neutrino mass

The relevant Feynman diagram of this modified type-II seesaw which gives rise to light neutrino masses is shown in Fig. 1. In this modified version of type-II seesaw, the conventional heavy triplet scalar Δ cannot generate Majorana masses for light neutrinos as the B − L quantum number of Δ is zero. However this super heavy scalar Δ can mix with the TeV scalar triplet ξ, once $\Phi_{\rm BL}$ acquires vev and breaks the $U(1)_{\rm B-L}$ symmetry spontaneously. By the virtue of the trilinear term of Δ with SM Higgs doublet H, it gets an induced vev after electroweak symmetry breaking similar to the case of traditional type-II seesaw. The induced vev acquired by Δ after EW phase transition is given by

$$\langle\Delta\rangle = v_\Delta \simeq -\frac{\mu_\Delta v_H^2}{2\sqrt{2}M_\Delta^2}. \quad (7)$$

Since ξ mixes with Δ after $U(1)_{\rm B-L}$ breaking, it also acquires an induced vev after EW symmetry breaking which is given by

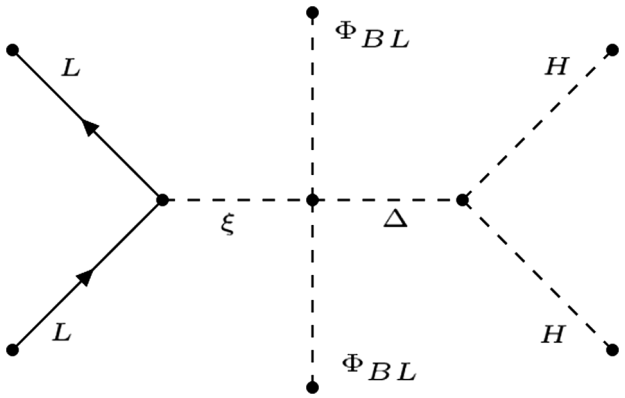

FIG. 1. Generation of neutrino mass through the modified type-II seesaw.

$$\langle \xi \rangle = v_\xi = -\frac{\lambda_P v_{\rm BL}^2}{4M_\xi^2} v_\Delta. \tag{8}$$

Assuming $\lambda_P v_{\rm BL}^2 \sim M_\xi^2$, we obtain $v_\Delta \simeq v_\xi$, even if ξ and Δ have several orders of magnitude difference in their masses.

As we know that, in the Standard Model the custodial symmetry ensures that the ρ parameter $\rho \equiv \frac{M_W^2}{M_Z^2 \cos^2\theta}$ is equal to 1 at tree level. However, in the present scenario, because of the presence of the triplet scalars, the form of the ρ parameter gets modified and is given by:

$$\rho = \frac{v_H^2 + 2v_\Delta^2 + 2v_\xi^2}{v_H^2 + 4v_\Delta^2 + 4v_\xi^2} \simeq \frac{1+4x^2}{1+8x^2}, \tag{9}$$

where $x = v_\Delta / v_H \simeq v_\xi / v_H$. According to the latest updates of the electroweak observables fits, the ρ parameter is constrained as $\rho = 1.00038 \pm 0.00020$ [64]. This implies that, corresponding to the constraints on the ρ parameter, we get an upper bound on the vev of the triplet ξ of order $\{1.650 - 2.962\}$ GeV.

After integrating out the heavy degrees of freedom in the Feynman diagram given in Fig. 1, we get the Majorana mass matrix of the light neutrinos to be

$$(M_\nu)_{ij} = Y_{ij}^\xi v_\xi = -Y_{ij}^\xi \frac{\lambda_P v_{\rm BL}^2}{4M_\xi^2} v_\Delta. \tag{10}$$

As $v_\Delta \simeq v_\xi \sim \mathcal{O}(1)$ GeV, we can get sub-eV neutrino masses by appropriately tuning the Yukawa couplings. Here it is worth noticing that the mixing between the super heavy triplet scalar Δ and the TeV scale scalar triplet ξ gives rise to the neutrino mass. Essentially this set-up can be thought of in an effective manner. After the $U(1)_{\rm B-L}$ breaking, ξ develops an effective trilinear coupling with the SM Higgs, i.e., $\mu_\xi \xi^\dagger HH$ where μ_ξ is given by $\mu_\xi = \mu_\Delta \langle \Phi_{\rm BL} \rangle^2 / M_\Delta^2$. And this effective coupling is similar to the conventional type-II seesaw which leads to the generation of neutrino mass in this scenario.

In Eq. (10), $(M_\nu)_{ij}$ is a complex 3×3 matrix and can be diagonalized by the PMNS matrix [65] for which the standard parametrization is given by:

$$U = \begin{pmatrix} c_{12}c_{13} & s_{12}c_{13} & s_{13}e^{-i\delta} \\ -s_{12}c_{23} - c_{12}s_{23}s_{13}e^{i\delta} & c_{12}c_{23} - s_{12}s_{23}s_{13}e^{i\delta} & s_{23}c_{13} \\ s_{12}s_{23} - c_{12}c_{23}s_{13}e^{i\delta} & -c_{12}s_{23} - s_{12}c_{23}s_{13}e^{i\delta} & c_{23}c_{13} \end{pmatrix} U_{ph}, \tag{11}$$

where $c_{ij} \equiv \cos\theta_{ij}$, $s_{ij} \equiv \sin\theta_{ij}$ and δ is the Dirac phase. Here U_{ph} is given by $U_{ph} = \mathrm{Diag}(1, e^{i\alpha_1/2}, e^{i\alpha_2/2})$ with $\alpha_{1,2}$ are the CP-violating Majorana phases.

From Eq. (10), we can write the couplings Y_{ij}^ξ as follows:

$$Y_{ij}^\xi = \frac{(M_\nu)_{ij}}{v_\xi} = \frac{1}{v_\xi} [U.M_\nu^{\rm diag}.U^T]_{ij}. \tag{12}$$

Neutrino oscillation experiments involving solar, atmospheric, accelerator, and reactor neutrinos are sensitive to the mass-squared differences and the mixing angles, and the value of these parameters in the 3σ range used in the analysis [64] are as follows.

$$\begin{aligned} &\Delta m_{\rm sol}^2 \equiv m_2^2 - m_1^2 \in [6.79 - 8.01] \times 10^{-5}\ \mathrm{eV}^2, \qquad |\Delta m_{atm}^2| \equiv |m_3^2 - m_1^2| \in [2.35, 2.54] \times 10^{-3}\ \mathrm{eV}^2 \\ &\sin^2\theta_{12} \in [0.27, 0.35], \qquad \sin^2\theta_{23} \in [0.43, 0.60], \qquad \sin^2\theta_{13} \in [0.019, 0.024]. \end{aligned} \tag{13}$$

Since the sign of Δm^2_{31} is undetermined, distinct neutrino mass hierarchies are possible. The case with $\Delta m^2_{31} > 0$ is referred to as *normal hierarchy* (NH) where $m_1 < m_2 < m_3$ and the case with $\Delta m^2_{31} < 0$ is known as *inverted hierarchy* (IH) where $m_3 < m_1 < m_2$. Information on the mass of the lightest neutrino and the Majorana phases cannot be obtained from neutrino oscillation experiments as the oscillation probabilities are independent of these parameters. Because of the general texture, the Yukawa couplings in Eq. (12) can facilitate charged lepton flavor violating (CLFV) decays and hence are constrained by the non-observation of such LFV processes at various experiments which we discuss in the Sec. II C.

B. Scalar masses and mixing

As already discussed in the Sec. II, the only significant mixing relevant for low energy phenomenological aspects is the mixing between H, ξ and Φ_3 since all other mixings are insignificant and can be neglected. In this section we only consider the light scalar sector, $V^{\mathbb{L}}(H, \xi, \Phi_3)$ which is relevant for low energy phenomenology.

The minimization conditions for the scalar potential are given by:

$$\begin{aligned}
\mu_H^2 &= \frac{1}{2}(\lambda_{H\Phi_3} v_3^2 + 2\lambda_H v_H^2 + v_\xi^2(\lambda_{\xi H} + \lambda'_{\xi H}) - 2\sqrt{2}\mu_\xi v_\xi) \\
M_\xi^2 &= \frac{1}{2}\left(-\lambda_{\xi\Phi_3} v_3^2 - v_H^2(\lambda_{\xi H} + \lambda'_{\xi H}) \right. \\
&\qquad \left. + \frac{\sqrt{2}\mu_\xi v_H^2}{v_\xi} - 2v_\xi^2(\lambda_\xi + \lambda'_\xi)\right) \\
\mu_{\Phi_3}^2 &= \frac{1}{2}(2\lambda_{\Phi_3} v_3^2 + \lambda_{H\Phi_3} v_H^2 + \lambda_{\xi\Phi_3} v_\xi^2).
\end{aligned} \tag{14}$$

The neutral CP even scalar mass terms of the Lagrangian can be expressed as:

$$\begin{aligned}
\mathcal{L}_{\text{mass}} &= \frac{1}{2}\begin{pmatrix} h_H & h_\xi & h_3 \end{pmatrix}\begin{pmatrix} 2\lambda_H v_H^2 & v_H v_\xi(\lambda_{\xi H} + \lambda'_{\xi H}) & \lambda_{H\Phi_3} v_3 v_H \\ v_H v_\xi(\lambda_{\xi H} + \lambda'_{\xi H}) & \frac{\mu_\xi v_H^2}{\sqrt{2} v_\xi} + 2v_\xi^2(\lambda_\xi + \lambda'_\xi) & \lambda_{\xi\Phi_3} v_3 v_\xi \\ \lambda_{H\Phi_3} v_3 v_H & \lambda_{\xi\Phi_3} v_3 v_\xi & 2\lambda_{\Phi_3} v_3^2 \end{pmatrix}\begin{pmatrix} h_H \\ h_\xi \\ h_3 \end{pmatrix} \\
&= \frac{1}{2}\begin{pmatrix} h_H & h_\xi & h_3 \end{pmatrix}\mathcal{M}^{\text{CP Even}}\begin{pmatrix} h_H \\ h_\xi \\ h_3 \end{pmatrix} \\
&= \frac{1}{2}\begin{pmatrix} H_1 & H_2 & H_3 \end{pmatrix}\begin{pmatrix} \mathcal{O}^T & \mathcal{M}^{\text{CP-Even}} & \mathcal{O} \end{pmatrix}\begin{pmatrix} H_1 \\ H_2 \\ H_3 \end{pmatrix} \\
&= \frac{1}{2}\begin{pmatrix} H_1 & H_2 & H_3 \end{pmatrix}\begin{pmatrix} m^2_{H_1} & 0 & 0 \\ 0 & m^2_{H_2} & 0 \\ 0 & 0 & m^2_{H_3} \end{pmatrix}\begin{pmatrix} H_1 \\ H_2 \\ H_3 \end{pmatrix}.
\end{aligned} \tag{15}$$

Here $\mathcal{O}$ is the orthogonal matrix which diagonalises the CP-even scalar mass matrix. Thus the flavor eigenstates and the mass eigenstates of these scalars are related by:

$$\begin{pmatrix} h_H \\ h_\xi \\ h_3 \end{pmatrix} = \begin{pmatrix} c_{12}c_{13} & c_{13}s_{12} & s_{13} \\ -c_{12}s_{13}s_{23} - c_{23}s_{12} & c_{12}c_{23} - s_{12}s_{13}s_{23} & c_{13}s_{23} \\ s_{12}s_{23} - c_{12}c_{23}s_{13} & -c_{12}s_{23} - c_{23}s_{12}s_{13} & c_{13}c_{23} \end{pmatrix}\begin{pmatrix} H_1 \\ H_2 \\ H_3 \end{pmatrix}, \tag{16}$$

where we abbreviated $\cos\beta_{ij} = c_{ij}$ and $\sin\beta_{ij} = s_{ij}$, with $\{ij{:}12, 13, 23\}$.

Apart from these three CP even physical states, H_1, H_2, and H_3 with masses $m_{H_1} = 125$ GeV (SM like Higgs), m_{H_2} and m_{H_3} respectively; the scalar sector has one massive CP odd scalar, A^0 of mass m_{A^0}, one massive singly charged scalar, $H^\pm$ of mass $m_{H^\pm}$ and one massive doubly charged scalar, $H^{\pm\pm}$ of mass $m_{H^{\pm\pm}}$. The masses of CP odd and charged states are given by:

$$m^2_{A^0} = \frac{\mu_\xi(v_H^2 + 4v_\xi^2)}{\sqrt{2}v_\xi}$$
$$m^2_{H^\pm} = \frac{2\sqrt{2}\mu_\xi v_H^2 - \lambda'_{\xi H} v_H^2 v_\xi - 2\lambda'_{\xi H} v_\xi^3 + 4\sqrt{2}\mu_\xi v_\xi^2}{4v_\xi}$$
$$m^2_{H^{\pm\pm}} = -\frac{\lambda'_{\xi H} v_H^2}{2} + \frac{\mu_\xi v_H^2}{\sqrt{2}v_\xi} - \lambda'_\xi v_\xi^2. \tag{17}$$

$U(1)_{\mathrm{B-L}}$ gauge boson mass: The Z_{BL} boson acquires mass through the vevs of Φ_{BL}, Φ_{12}, Φ_3 which are charged under $U(1)_{\mathrm{B-L}}$ and is given by:

$$M^2_{Z_{\mathrm{BL}}} \simeq g^2_{\mathrm{BL}}(v^2_{\mathrm{BL}} + 64v^2_{12} + 100v^2_3). \tag{18}$$

The quartic couplings of scalars are expressed in term of physical masses, vevs and mixing as:

$$\begin{aligned}
\lambda_H &= \frac{c_{13}^2(c_{12}^2 m_{H_1}^2 + m_{H_2}^2 s_{12}^2) + m_{H_3}^2 s_{13}^2}{2v_H^2} \\
\lambda_{\xi H} &= \frac{c_{13}s_{13}s_{23}(-c_{12}^2 m_{H_1}^2 - m_{H_2}^2 s_{12}^2 + m_{H_3}^2) + c_{12}c_{13}c_{23}s_{12}(m_{H_2}^2 - m_{H_1}^2)}{v_H v_\xi} + \frac{4m^2_{H^\pm}}{v_H^2 + 2v_\xi^2} - \frac{2m^2_{A^0}}{v_H^2 + 4v_\xi^2} \\
\lambda_\xi &= \frac{s_{23}^2(s_{13}^2(c_{12}^2 m_{H_1}^2 + m_{H_2}^2 s_{12}^2) + c_{13}^2 m_{H_3}^2) + c_{23}^2(c_{12}^2 m_{H_2}^2 + m_{H_1}^2 s_{12}^2) - 4m^2_{H^\pm} + 2m^2_{H^{\pm\pm}}}{2v_\xi^2} \\
&\quad + \frac{2c_{12}c_{23}s_{12}s_{13}s_{23}(m_{H_1} - m_{H_2})(m_{H_1} + m_{H_2})}{2v_\xi^2} + \frac{4m^2_{H^\pm}}{v_H^2 + 2v_\xi^2} - \frac{2m^2_{A^0}}{v_H^2 + 4v_\xi^2} \\
\lambda'_\xi &= -\frac{m^2_{A^0} - m^2_{H^{\pm\pm}} - 2m^2_{H^\pm}}{v_\xi^2} + \frac{4m^2_{A^0}}{v_H^2 + 4v_\xi^2} - \frac{4m^2_{H^\pm}}{v_H^2 + 2v_\xi^2} \\
\lambda'_{\xi H} &= \frac{4m^2_{A^0}}{v_H^2 + 4v_\xi^2} - \frac{4m^2_{H^\pm}}{v_H^2 + 2v_\xi^2} \\
\mu_\xi &= \frac{\sqrt{2}m^2_{A^0} v_\xi}{v_H^2 + 4v_\xi^2} \\
\lambda_{\Phi_3} &= \frac{m_{H_1}^2(c_{12}c_{23}s_{13} - s_{12}s_{23})^2 + m_{H_2}^2(c_{12}s_{23} + c_{23}s_{12}s_{13})^2 + c_{13}^2 c_{23}^2 m_{H_3}^2}{2v_3^2} \\
\lambda_{H\Phi_3} &= \frac{c_{13}c_{23}s_{13}(-c_{12}^2 m_{H_1}^2 - m_{H_2}^2 s_{12}^2 + m_{H_3}^2) + c_{12}c_{13}s_{12}s_{23}(m_{H_1} - m_{H_2})(m_{H_1} + m_{H_2})}{v_3 v_H} \\
\lambda_{\xi\Phi_3} &= \frac{m_{H_1}^2(c_{12}s_{13}s_{23} + c_{23}s_{12})(c_{12}c_{23}s_{13} - s_{12}s_{23}) - m_{H_2}^2(c_{12}s_{23} + c_{23}s_{12}s_{13})(c_{12}c_{23} - s_{12}s_{13}s_{23})}{v_3 v_\xi} \\
&\quad + \frac{c_{13}^2 c_{23} m_{H_3}^2 s_{23}}{v_3 v_\xi}.
\end{aligned} \tag{19}$$

1. Constraints on scalar sector

As already discussed in Sec. II A, based on the measurement of the ρ parameter $\rho = 1.00038 \pm 0.00020$ [64], the triplet ξ vev v_ξ can have an upper bound of order $\{1.650 - 2.962\}$ GeV. Also the mixing angle between the SM Higgs and the triplet scalar is constrained from Higgs decay measurement. As obtained by [66], this mixing angle $\sin\beta_{12}$ is bounded above, in particular, $\sin\beta_{12} \lesssim 0.05$ to be consistent with experimental observation of $H_1 \to WW^*$ [47,66]. There are similar bounds on singlet scalar mixing with the SM Higgs boson. Such bounds come from both theoretical and experimental constraints [67–69]. The upper bound on singlet scalar-SM Higgs mixing angle $\sin\beta_{13}$ comes form W boson mass correction [70] at NLO. For 250 GeV $< m_{H_3} <$ 850 GeV, $\sin\beta_{13}$ is constrained to be $\sin\beta_{13} < 0.2 - 0.3$ where m_{H_3} is the mass of the third physical Higgs.

For our further discussion, we consider the following benchmark points where all the above mentioned constraints are satisfied as well as the quartic couplings mentioned in Eq. (19) are within the unitarity and perturbativity limit.

$$\{m_{H_2} = 331.779, \quad m_{H_3} = 366.784, \quad m_{A^0} = 331.779, \quad m_{H^\pm} = 369.841, \quad m_{H^{\pm\pm}} = 404.343$$
$$v_\xi = 2.951 \text{ (in GeV)}; \quad s_{12} = 0.03, \quad s_{23} = s_{13} = 0.01\}. \tag{20}$$

This parameter choice in Eq. (20) is for definiteness. It is not exhaustive. One can consider another set of parameters in Eq. (20), without changing any of the consequences in the dark sector that we study here.

C. Charged lepton flavor violation

Charged lepton flavor violating (CLFV) decay is a promising process to study from beyond standard model (BSM) physics point of view. In the SM, such a process occurs at one-loop level and is suppressed by the smallness of neutrino masses, much beyond the current experimental sensitivity. Therefore, any future observation of such LFV decays like $\mu \to 3e$ or $\mu \to e\gamma$ will definitely be a signature of new physics beyond the SM. In our model such CLFV decays can occur at tree level mainly mediated via the triplet scalar $H^{\pm\pm}$ and at one-loop level mediated by $H^{\pm\pm}$ and $H^\pm$.

The branching ratio for $\mu \to 3e$ process which can occur at tree level is given by:

$$\text{Br}(\mu \to 3e) = \frac{|Y^\xi_{\mu e}|^2 |Y^\xi_{ee}|^2}{4G_F^2 m^4_{H^{\pm\pm}}} \text{Br}(\mu \to e\bar{\nu}\nu), \tag{21}$$

where $\text{Br}(\mu \to e\bar{\nu}\nu) \simeq 100\%$.

Similarly, the branching ratio for $\mu \to e\gamma$ which can take place at loop level is given by (with $m_{H^\pm} \simeq m_{H^{\pm\pm}}$):

$$\text{Br}(\mu \to e\gamma) \simeq \frac{27\alpha |(Y^{\xi\dagger} Y^\xi)_{e\mu}|^2}{64\pi G_F^2 m^4_{H^{\pm\pm}}} \text{Br}(\mu \to e\bar{\nu}\nu). \tag{22}$$

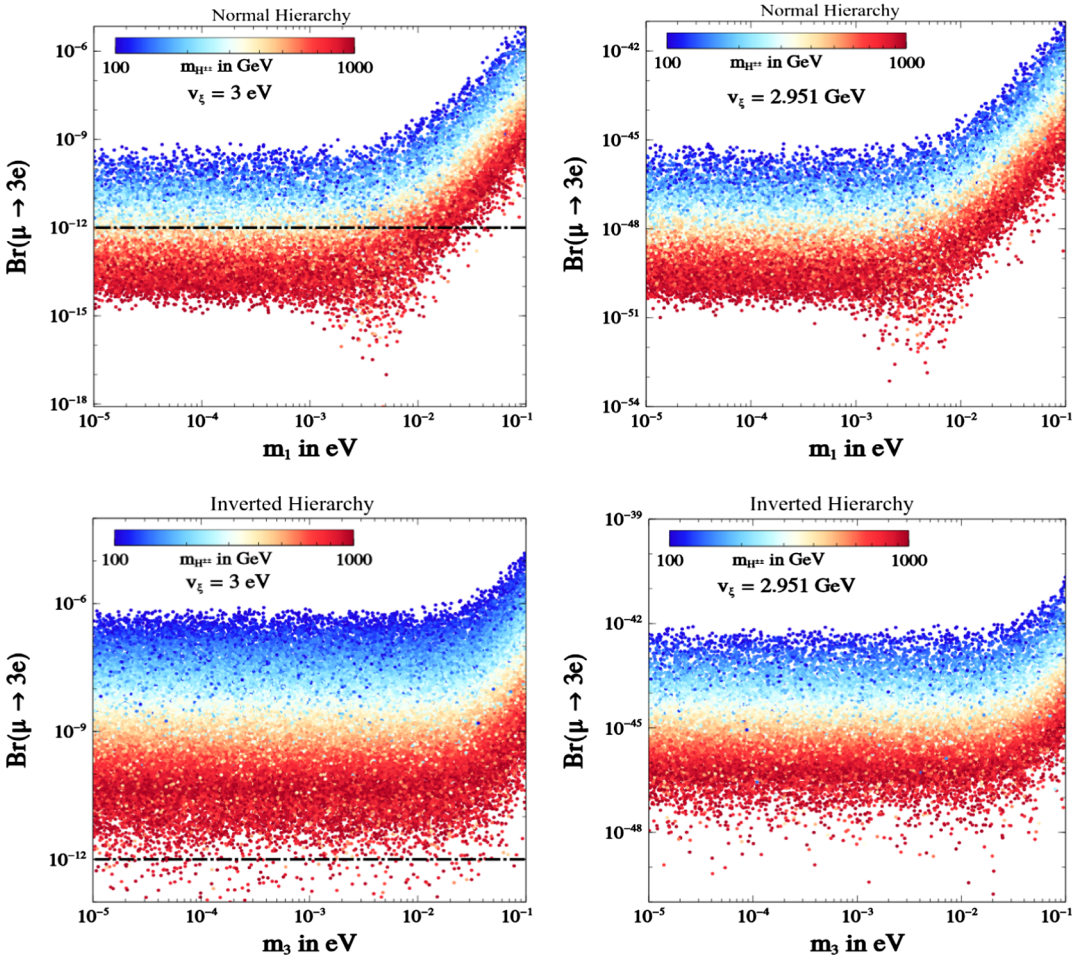

FIG. 2. $\text{Br}(\mu \to 3e)$ as a function of the lightest neutrino mass for both normal and inverted hierarchy. The color code shows the mass of doubly charged scalar $m_{H^{\pm\pm}}$. The black dotted line shows the current bound from [72].

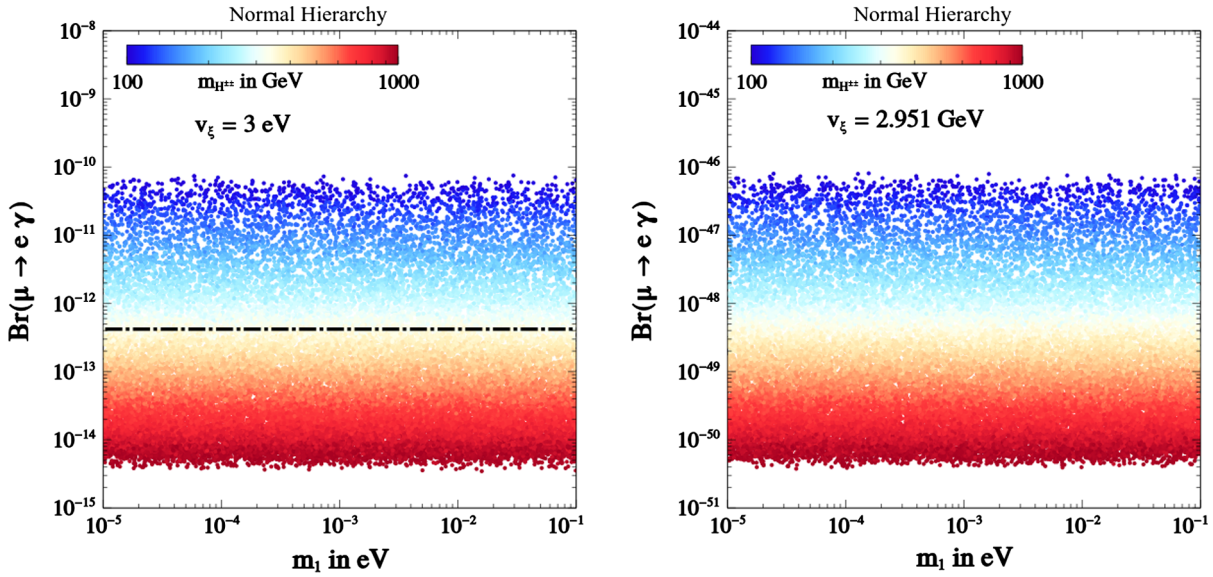

FIG. 3. $\mathrm{Br}(\mu \to e\gamma)$ as a function of the lightest neutrino mass for normal hierarchy. The color code shows the mass of doubly charged scalar $m_{H^{\pm\pm}}$. The black dotted line shows the current bound from [73].

We have shown the $\mathrm{Br}(\mu \to 3e)$ as a function of the lightest neutrino mass for both normal and inverted hierarchy of neutrino mass spectrum in the upper and lower panel of Fig. 2 and $\mathrm{Br}(\mu \to e\gamma)$ has been shown in Fig. 3 for only normal hierarchy as $\mathrm{Br}(\mu \to e\gamma)$ is not so sensitive to the neutrino mass spectrum as pointed out in [43,71]. The left and right panel figures of Figs. 2 and 3 are for $v_\xi = 3$ eV and $v_\xi = 2.951$ GeV respectively. Clearly for v_ξ in the eV scale, the constraints from the CLFV can rule out higher values of Yukawa couplings and light $m_{H^{\pm\pm}}$. However if v_ξ is in the GeV scale, which is the case for our analysis, (such that $H^{\pm\pm}$ dominantly decays to $W^\pm W^\pm$ details of which are given in Appendix B) which is crucial for the collider study of H^{++} in our model discussed in Sec. V, the $\mathrm{Br}(\mu \to 3e)$ and $\mathrm{Br}(\mu \to e\gamma)$ are far below the present and future sensitivity of these experiments and hence these bounds do not affect our parameter space.

III. DARK MATTER

The $U(1)_{\mathrm{B-L}}$ gauge symmetry gets spontaneously broken down by the vev of Φ_{12}, Φ_{BL} and Φ_3 to a remnant $\mathcal{Z}_2$ symmetry under which the dark sector fermions: χ_{i_R} ($i = e$, μ, τ) are assumed to be odd, while all other particles transforms trivially. As a result, the lightest among these fermions becomes a viable candidate of DM and can give rise to the observed relic density by thermal freeze-out mechanism.

A. The dark sector fermions and their interactions

From Eq. (2), the mass matrix for χ_{i_R} ($i = e, \mu, \tau$) in the effective theory can be written as:

$$-\mathcal{L}_\chi^{\mathrm{mass}} = \frac{1}{2}\left(\overline{(\chi_{e_R})^c} \quad \overline{(\chi_{\mu_R})^c} \quad \overline{(\chi_{\tau_R})^c}\right)\mathcal{M}\begin{pmatrix}\chi_{e_R}\\ \chi_{\mu_R}\\ \chi_{\tau_R}\end{pmatrix}, \tag{23}$$

where

$$\mathcal{M} = \frac{1}{\sqrt{2}}\begin{pmatrix} Y_{11}v_{12} & Y_{12}v_{12} & Y_{13}v_{\mathrm{BL}} \\ Y_{12}v_{12} & Y_{22}v_{12} & Y_{23}v_{\mathrm{BL}} \\ Y_{13}v_{\mathrm{BL}} & Y_{23}v_{\mathrm{BL}} & Y_{33}v_3 \end{pmatrix} = \begin{pmatrix} [M_{12}] & [M'] \\ [M']^T & M_3 \end{pmatrix}. \tag{24}$$

Here M_{12}, M', M_3 are

$$M_{12} = \frac{1}{\sqrt{2}}\begin{pmatrix} Y_{11}v_{12} & Y_{12}v_{12} \\ Y_{12}v_{12} & Y_{22}v_{12}\end{pmatrix}, \quad M' = \frac{1}{\sqrt{2}}\begin{pmatrix} Y_{13}v_{\mathrm{BL}} \\ Y_{23}v_{\mathrm{BL}}\end{pmatrix}, \quad M_3 = \frac{1}{\sqrt{2}}(Y_{33}v_3).$$

To capture the coannihilation effect in the dark sector in a simplest way, we assume

$$Y_{11} = Y_{22}, \qquad Y_{13} = Y_{23} \quad \text{and} \quad Y_{12} \ll 1. \tag{25}$$

With this assumption two of the dark sector fermions χ_e and χ_μ become almost degenerate and their mixing with the DM χ_τ will be defined by a single mixing angle. Moreover, the mass splitting between the DM and NLSP (next to lightest stable particle) will be unique as we discuss below. However, relaxation of this assumption (25) will lead to two mass splittings and three mixing angles in the dark

sector, which make our analysis unnecessarily complicated without implying any new features. So without loss of generality we assert to Eq. (25) in the following analysis.

Using Eq. (25), the above Majorana fermion mass matrix $\mathcal{M}$ can be exactly diagonalized by an orthogonal rotation $\mathcal{R} = \mathcal{R}_{13}(\theta).\mathcal{R}_{23}(\theta_{23} = 0).\mathcal{R}_{12}(\theta_{12} = \frac{\pi}{4})$ which is essentially characterized by only one parameter θ [74]. So we diagonalized the mass matrix $\mathcal{M}$ as $\mathcal{R}.\mathcal{M}.\mathcal{R}^T = \mathcal{M}_{\text{Diag}}$., where the $\mathcal{R}$ is given by:

$$\mathcal{R} = \begin{pmatrix} \frac{1}{\sqrt{2}}\cos\theta & \frac{1}{\sqrt{2}}\cos\theta & \sin\theta \\ -\frac{1}{\sqrt{2}} & \frac{1}{\sqrt{2}} & 0 \\ -\frac{1}{\sqrt{2}}\sin\theta & -\frac{1}{\sqrt{2}}\sin\theta & \cos\theta \end{pmatrix}. \tag{26}$$

The rotation parameter θ required for the diagonalization is given by:

$$\tan 2\theta = \frac{2\sqrt{2}Y_{13}v_{\text{BL}}}{(Y_{11}+Y_{12})v_{12} - Y_{33}v_3}. \tag{27}$$

Thus the physical states of the dark sector are $\chi_i = \frac{\chi_{i_R} + (\chi_{i_R})^c}{\sqrt{2}}$ and are related to the flavor eigenstates by the following linear combinations:

$$\begin{aligned} \chi_{1_R} &= \frac{1}{\sqrt{2}}\cos\theta\chi_{e_R} + \frac{1}{\sqrt{2}}\cos\theta\chi_{\mu_R} + \sin\theta\chi_{\tau_R} \\ \chi_{2_R} &= -\frac{1}{\sqrt{2}}\chi_{e_R} + \frac{1}{\sqrt{2}}\chi_{\mu_R} \\ \chi_{3_R} &= -\frac{1}{\sqrt{2}}\sin\theta\chi_{e_R} - \frac{1}{\sqrt{2}}\sin\theta\chi_{\mu_R} + \cos\theta\chi_{\tau_R}. \end{aligned} \tag{28}$$

And the corresponding mass eigenvalues are given by:

$$\begin{aligned} M_1 &= \frac{1}{2\sqrt{2}}\left[(Y_{11}+Y_{12})v_{12} + Y_{33}v_3 + \sqrt{((Y_{11}+Y_{12})v_{12} - Y_{33}v_3)^2 + 8(Y_{13}v_{\text{BL}})^2}\right] \\ M_2 &= \frac{1}{\sqrt{2}}(Y_{11}-Y_{12})v_{12} \\ M_3 &= \frac{1}{2\sqrt{2}}\left[(Y_{11}+Y_{12})v_{12} + Y_{33}v_3 - \sqrt{((Y_{11}+Y_{12})v_{12} - Y_{33}v_3)^2 + 8(Y_{13}v_{\text{BL}})^2}\right]. \end{aligned} \tag{29}$$

Here it is worthy to mention that in the limit of $Y_{13} \to 0$, i.e., $\theta \to 0$, we get the mass eigenvalues of the DM particles as $M_{1,2} = \frac{1}{\sqrt{2}}(Y_{11} \pm Y_{12})v_{12}$ and $M_3 = \frac{1}{\sqrt{2}}Y_{33}v_3$ and the corresponding mass eigenstates are $\chi_{1_R,2_R} = \frac{1}{\sqrt{2}}(\chi_{\mu_R} \pm \chi_{e_R})$ and $\chi_{3_R} = \chi_{\tau_R}$. If we assume that the off diagonal Yukawa couplings: i.e., $Y_{12}, Y_{13} \ll 1$, then χ_1 and χ_2 become almost degenerate (i.e., $M_1 \simeq M_2$).

We assume χ_3 to be the lightest state which represents the DM candidate, while χ_1 and χ_2 are NLSPs which are almost degenerate. Using the relation $\mathcal{R}.\mathcal{M}.\mathcal{R}^T = \mathcal{M}_{\text{Diag}}$., one can express the following relevant parameters in terms of the physical masses M_1, M_3 and the mixing angle $\sin\theta$ as

$$\begin{aligned} v_3 &= \frac{\sqrt{2}}{Y_{33}}(M_1\sin^2\theta + M_3\cos^2\theta) \\ v_{12} &= \frac{\sqrt{2}}{Y_{33}+Y_{12}}(M_1\cos^2\theta + M_3\sin^2\theta) \\ Y_{13} &= \frac{\Delta M\sin 2\theta}{2v_{\text{BL}}}, \end{aligned} \tag{30}$$

where ΔM is the mass splitting between the DM and NLSPs, i.e., $\Delta M = M_1 - M_3$.

The gauge coupling g_{BL} can be expressed as

$$g_{\text{BL}} \simeq \frac{M_{Z_{\text{BL}}}}{\sqrt{(v_{\text{BL}}^2 + 64v_{12}^2 + 100v_3^2)}}. \tag{31}$$

The flavor eigenstates can be expressed in terms of the physical eigenstates as follows:

$$\begin{aligned} \chi_{e_R} &= \frac{1}{\sqrt{2}}\cos\theta\chi_{1_R} - \frac{1}{\sqrt{2}}\chi_{2_R} - \frac{1}{\sqrt{2}}\sin\theta\chi_{3_R} \\ \chi_{\mu_R} &= \frac{1}{\sqrt{2}}\cos\theta\chi_{1_R} + \frac{1}{\sqrt{2}}\chi_{2_R} - \frac{1}{\sqrt{2}}\sin\theta\chi_{3_R} \\ \chi_{\tau_R} &= \sin\theta\chi_{1_R} + \cos\theta\chi_{3_R}. \end{aligned} \tag{32}$$

1. DM interactions

The Yukawa and gauge interactions of DM relevant for the calculation of relic density can be written in the physical eigenstates as follows:

$$\begin{aligned}\mathcal{L}_{\text{Yuk.}} &= Y_{33}h_3\overline{(\chi_{\tau_R})^c}\chi_{\tau_R}\\ &= Y_{33}[(s_{12}s_{23}-c_{12}c_{23}s_{13})H_1-(c_{12}s_{23}+c_{23}s_{12}s_{13})H_2+(c_{13}c_{23})H_3]\overline{(\chi_{\tau_R})^c}\chi_{\tau_R}\\ &= Y_{33}[(s_{12}s_{23}-c_{12}c_{23}s_{13})H_1-(c_{12}s_{23}+c_{23}s_{12}s_{13})H_2+(c_{13}c_{23})H_3]\\ &\quad\times[\sin^2\theta\overline{(\chi_{1_R})^c}\chi_{1_R}+\cos^2\theta\overline{(\chi_{3_R})^c}\chi_{3_R}+\sin\theta\cos\theta(\overline{(\chi_{1_R})^c}\chi_{3_R}+\overline{(\chi_{3_R})^c}\chi_{1_R})]\end{aligned} \tag{33}$$

and

$$\begin{aligned}\mathcal{L}_{Z_{\text{BL}}} &= g_{\text{BL}}[(4\cos^2\theta+5\sin^2\theta)\overline{\chi_{1_R}}\gamma^\mu\chi_{1_R}+4\overline{\chi_{2_R}}\gamma^\mu\chi_{2_R}\\ &\quad+(4\sin^2\theta+5\cos^2\theta)\overline{\chi_{3_R}}\gamma^\mu\chi_{3_R}\\ &\quad+\cos\theta\sin\theta(\overline{\chi_{1_R}}\gamma^\mu\chi_{3_R}+\overline{\chi_{3_R}}\gamma^\mu\chi_{1_R})](Z_{\text{BL}})_\mu.\end{aligned} \tag{34}$$

Note that there is no coannihilation of χ_3 with χ_2. The dominant annihilation and coannihilation channels for DM are shown in Figs. 4–7.

B. Relic abundance of DM

The DM phenomenology is mainly governed by the following independent parameters:

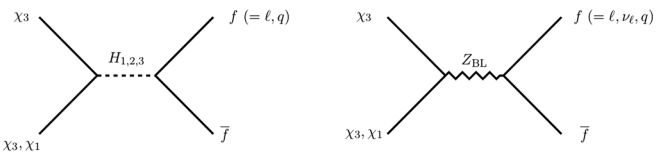

FIG. 4. Feynman diagrams for DM annihilation and coannihilations: $\chi_3\chi_{3,1}\to f\bar{f}$.

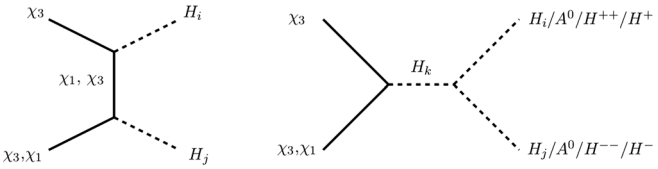

FIG. 5. Feynman diagrams for DM annihilation and coannihilations: $\chi_3\chi_{3,1}\to H_iH_j, A^0A^0\,H^+H^-, H^{++}H^{--}$ $(i,j,k=1,2,3)$.

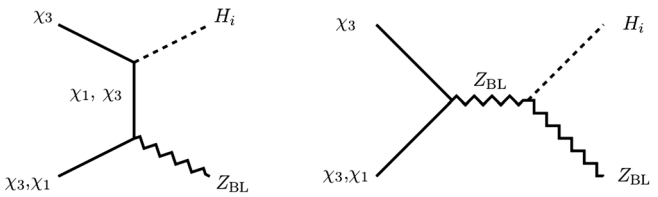

FIG. 6. Feynman diagrams for DM annihilation and coannihilation: $\chi_3\chi_{3,1}\to H_iZ_{\text{BL}}$ $(i=1,2,3)$.

$$\begin{aligned}\{M_3\equiv M_{\text{DM}},\Delta M\equiv(M_1-M_3)\\ \simeq(M_2-M_3),\sin\theta,Y_{33},M_{Z_{\text{BL}}}\}.\end{aligned} \tag{35}$$

while the other independent parameters that are kept fixed are: $v_{\text{BL}}=10$ TeV, $Y_{12}=10^{-6}$, and the dependent parameters are g_{BL}, v_3, v_{12} and Y_{13} as mentioned in Eqs. (30) and (31). Depending on the relative magnitudes of these parameters, DM relic can be generated dominantly by annihilation or coannihilation or a combination of both. The variation of the effective couplings, involved in the annihilation and coannihilation processes of DM as given in Eqs. (33) and (34), with the dark fermions mixing angle $\sin\theta$, which plays a crucial role in DM phenomenology, can be visualized as shown in Fig. 8. Clearly in the limit $\sin\theta\to 0$, the Yukawa coupling involved DM annihilation processes ($\propto Y_{33}\cos^2\theta$) dominate, whereas for $\sin\theta\to 1$, the Yukawa coupling involved coannihilation processes ($\propto Y_{33}\sin^2\theta, Y_{33}\sin\theta\cos\theta$) dominate and play a crucial role in determining the correct relic density. The gauge coupling involved annihilation and coannihilation processes are almost comparable irrespective of the values of $\sin\theta$.

The relic density of DM in this scenario can be estimated by solving the Boltzmann equation in the following form:

$$\frac{dn}{dt}+3Hn=-\langle\sigma v\rangle_{\text{eff}}(n^2-n_{eq}^2), \tag{36}$$

where n denotes the relic of dark sector fermions, i.e., $n=n_{\chi_1}+n_{\chi_2}+n_{\chi_3}$ and $n_{eq}=g(M_{\text{DM}}T/2\pi)^{3/2}\exp(-M_{\text{DM}}/T)$ is equilibrium distribution. Here $g=g_1+g_2+g_3$ where g_3, g_1, g_2 are the internal degrees of freedom of χ_3, χ_1, and χ_2 respectively. The DM freezes out giving us the thermal relic depending on $\langle\sigma v\rangle_{\text{eff}}$, which takes into account all number changing process listed in Figs. 4–7. This can be written as:

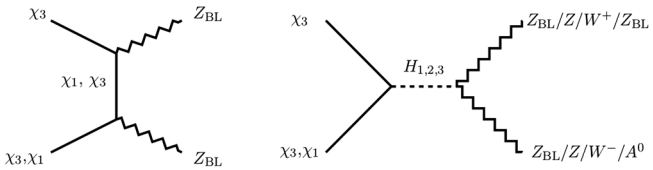

FIG. 7. Feynman diagrams for DM annihilation and coannihilation: $\chi_3\chi_{3,1}\to Z_{\text{BL}}Z_{\text{BL}}; ZZ; W^+W^-$ and $Z_{\text{BL}}A^0$.

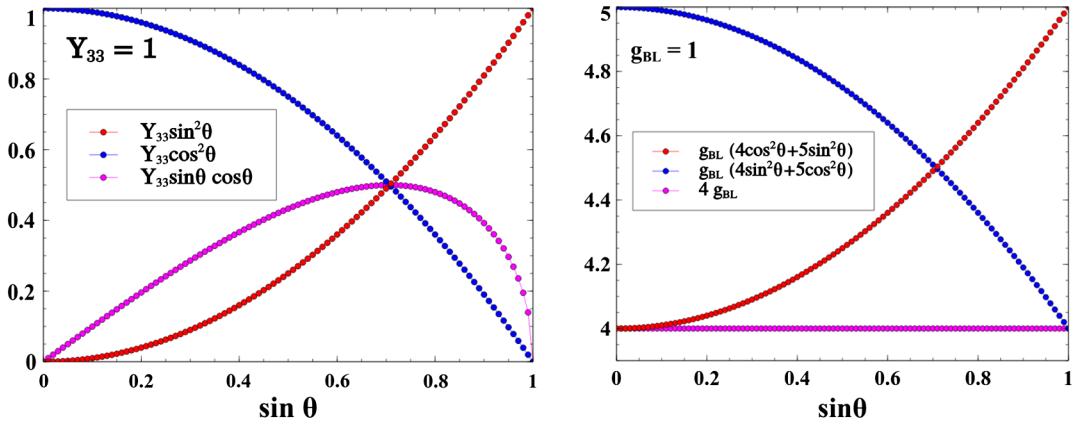

FIG. 8. Left: the effective couplings in Yukawa interactions given in Eq. (33). Right: the effective couplings in gauge interactions given in Eq. (34).

$$\langle\sigma v\rangle_{\rm eff} = \frac{g_3^2}{g_{\rm eff}^2}\langle\sigma v\rangle_{\chi_3\chi_3} + \frac{2g_3g_1}{g_{\rm eff}^2}\langle\sigma v\rangle_{\chi_3\chi_1}\left(1+\frac{\Delta M}{M_{\rm DM}}\right)^{\frac{3}{2}}\exp\left(-x\frac{\Delta M}{M_{\rm DM}}\right) + \frac{g_1^2}{g_{\rm eff}^2}\langle\sigma v\rangle_{\chi_1\chi_1}\left(1+\frac{\Delta M}{M_{\rm DM}}\right)^{3}\exp\left(-2x\frac{\Delta M}{M_{\rm DM}}\right) + \frac{g_2^2}{g_{\rm eff}^2}\langle\sigma v\rangle_{\chi_2\chi_2}\left(1+\frac{\Delta M}{M_{\rm DM}}\right)^{3}\exp\left(-2x\frac{\Delta M}{M_{\rm DM}}\right). \tag{37}$$

Here $g_{\rm eff}$ is the effective degrees of freedom which can be expressed as,

$$g_{\rm eff} = g_3 + g_1\left(1+\frac{\Delta M}{M_{\rm DM}}\right)^{\frac{3}{2}}\exp\left(-x\frac{\Delta M}{M_{\rm DM}}\right) + g_2\left(1+\frac{\Delta M}{M_{\rm DM}}\right)^{\frac{3}{2}}\exp\left(-x\frac{\Delta M}{M_{\rm DM}}\right) \tag{38}$$

and the dimensionless parameter x is defined as $x = \frac{M_{\rm DM}}{T} = \frac{M_3}{T}$.

Equation (37) can be written in a precise form for convenience in discussion as:

$$\langle\sigma v\rangle_{\rm eff} = \frac{g_3^2}{g_{\rm eff}^2}\langle\sigma v\rangle_{\chi_3\chi_3} + \langle\sigma v\rangle_{\chi_3\chi_1} f(\Delta M, M_{\rm DM}) + \langle\sigma v\rangle_{\chi_1\chi_1} h_1(\Delta M, M_{\rm DM}) + \langle\sigma v\rangle_{\chi_2\chi_2} h_2(\Delta M, M_{\rm DM}), \tag{39}$$

where f, h_1, and h_2 are the factors multiplied to the coannihilation cross sections which are functions of ΔM and $M_{\rm DM}$.

The relic density of the DM (χ_3) then can be given by [75–77]:

$$\Omega_{\chi_3}h^2 = \frac{1.09\times10^9\ {\rm GeV}^{-1}}{g_*^{1/2}M_{\rm Pl}}\frac{1}{J(x_f)}, \tag{40}$$

where $g_* = 106.7$ and $J(x_f)$ is given by

$$J(x_f) = \int_{x_f}^{\infty}\frac{\langle\sigma v\rangle_{\rm eff}}{x^2}dx. \tag{41}$$

Here $x_f = \frac{M_{\rm DM}}{T_f}$, and T_f denotes the freeze-out temperature of the DM χ_3. We may note here that for correct relic $x_f \simeq 25$.

It is worth mentioning here that we used the package MicrOmegas [78] for computing annihilation cross section and relic density, after generating the model files using LanHEP [79].

C. Parameter space scan

To understand the DM relic density and the specific role of the model parameters in giving rise to the observed relic density, we performed several analyses and scan for allowed parameter space. As discussed in Sec. III A, the important relevant parameters controlling the relic abundance of DM are: the mass of DM ($M_{\rm DM}$), mass splitting (ΔM) between the DM (χ_3) and the next to lightest stable particle (χ_2 and χ_1 as $M_1 \simeq M_2$), and the mixing angle $\sin\theta$. Apart from these three, another crucial parameter that has a noteworthy effect on DM relic, as well as other phenomenological aspects, is the Yukawa coupling Y_{33}. We also keep the B − L gauge boson mass ($M_{Z_{\rm BL}}$) as a free parameter. The dependent parameters have already been mentioned in Eqs. (30) and (31). The other parameters that

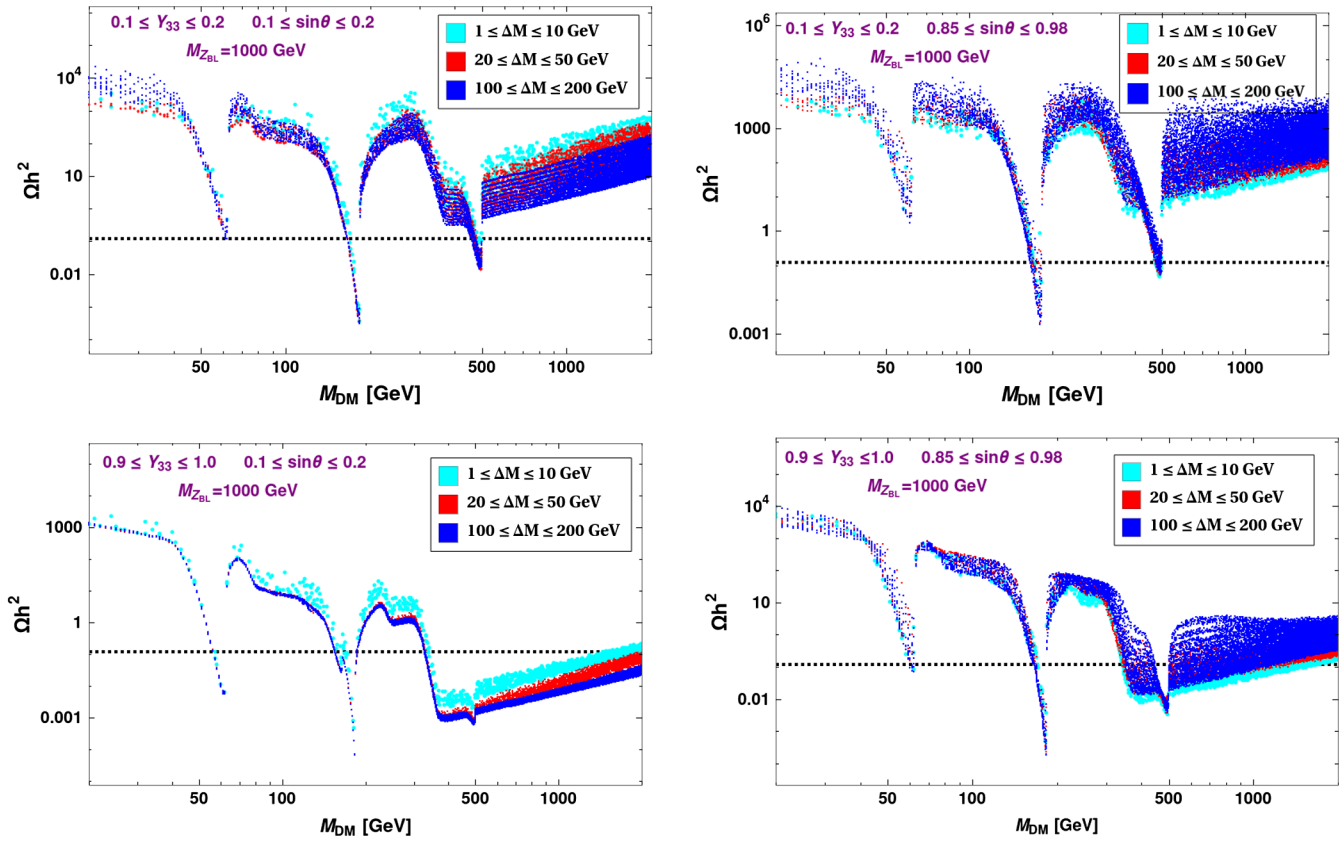

FIG. 9. Variation of relic density as a function of DM mass. Other parameters are kept fixed as mentioned inset of each figure.

are kept fixed judiciously during the analysis are $v_{\rm BL} = 10$ TeV and $Y_{12} = 10^{-6}$. The masses and mixing of Higgses are fixed as per Eq. (20). We show the variation of relic density of DM χ_3 in Fig. 9 as a function of its mass $M_{\rm DM}$ for different choices of ΔM: 1–10 GeV, 20–50 GeV and 100–200 GeV shown by different colored points as mentioned in the inset of the figure. The dips in the relic density plots are essentially due to resonances corresponding to SM-Higgs, second Higgs and $Z_{\rm BL}$ gauge bosons respectively. In the top-left and top-right panel, Y_{33} is varied in a range $0.1 \leq Y_{33} \leq 0.2$ whereas in the bottom-left and bottom-right panel it is varied in an interval $0.9 \leq Y_{33} \leq 1$. Clearly as Y_{33} increases, the effective annihilation cross section increases which decreases the relic density.

We can also analyze the effect of mixing angle $\sin\theta$ and mass splitting (ΔM) from the results in Fig. 9. As already mentioned, the parameter which decides the contribution of coannihilations of DM to the relic density is $\sin\theta$ which can be understood by looking at Eqs. (33) and (34). If $\sin\theta$ is small then the contribution from annihilation of DM will dominate overall coannihilation effects but for larger $\sin\theta$, coannihilation contributions will be more as compared to the annihilations. The value of $\sin\theta$ predominantly decides the relative contribution of annihilation and coannihilations of DM for the calculation of relic density. However the mass-splitting also plays a crucial role in the effect of annihilations and coannihilations of DM. With increase in mass-splitting, the contribution from coannihilation processes gradually debilitates and becomes less effective. This is evident from Tables II, III, and IV.

In the top and bottom right panel of Fig. 9, $\sin\theta$ is randomly varied in a range $0.85 \leq \sin\theta \leq 0.98$ for two different ranges of Y_{33}. For such a large $\sin\theta$, DM annihilates very weakly, so the coannihilations essentially decides the effective annihilation cross section and hence the relic density. This means in Eq. (37), the first term is negligible as compared to the other terms. In such a case, as ΔM increases, these coannihilations become less and less effective thus decreasing the effective annihilation cross section hence increasing the relic density. This trend is clearly observed in the right panel plots of Fig. 9. The effect of mass splitting in such a case can also be understood by looking at the right panel of Fig. 10 where the multiplying functions (mentioned as $f(\Delta M)$ and $h(\Delta M)$) in the coannihilation terms of the effective annihilation cross section in Eq. (39), are plotted as a function of mass-splitting ΔM. As ΔM increases, these factors decreases drastically consequently decreasing the overall effective annihilation cross section and hence increasing the relic density of DM.

TABLE II. Dominant annihilation and coannihilation channels for $\sin\theta = 0.1$.

	Dominant number changing processes		
$M_{\rm DM}$ in GeV	$\Delta M = 1$	$\Delta M = 10$	$\Delta M = 100$
30	$\chi_3\chi_3 \to f\bar{f}(76)\%$ $\chi_{1,2}\chi_{1,2} \to f\bar{f}(12)\%$	$\chi_3\chi_3 \to f\bar{f}(100)\%$	$\chi_3\chi_3 \to f\bar{f}(100)\%$
100	$\chi_3\chi_3 \to W^+W^-(51\%)$ $\chi_3\chi_3 \to ZZ(19\%)$ $\chi_3\chi_3 \to f\bar{f}(13\%)$	$\chi_3\chi_3 \to W^+W^-(58\%)$ $\chi_3\chi_3 \to ZZ(22\%)$ $\chi_3\chi_3 \to f\bar{f}(20\%)$	$\chi_3\chi_3 \to W^+W^-(58\%)$ $\chi_3\chi_3 \to ZZ(22\%)$ $\chi_3\chi_3 \to f\bar{f}(20\%)$
300	$\chi_3\chi_3 \to H_{1,3}H_3(19\%)$ $\chi_3\chi_3 \to f\bar{f}(39\%)$ $\chi_2\chi_2 \to f\bar{f}(20\%)$ $\chi_1\chi_1 \to f\bar{f}(12\%)$	$\chi_3\chi_3 \to H_{1,3}H_3(28\%)$ $\chi_3\chi_3 \to f\bar{f}(60\%)$	$\chi_3\chi_3 \to H_{1,3}H_3(31\%)$ $\chi_3\chi_3 \to f\bar{f}(64\%)$
1000	$\chi_3\chi_3 \to Z_{\rm BL}H_3(49\%)$ $\chi_2\chi_2 \to Z_{\rm BL}H_3(23\%)$ $\chi_1\chi_1 \to Z_{\rm BL}H_3(22\%)$	$\chi_3\chi_3 \to Z_{\rm BL}H_3(75\%)$ $\chi_2\chi_2 \to Z_{\rm BL}H_3(10\%)$ $\chi_1\chi_1 \to Z_{\rm BL}H_3(9\%)$	$\chi_3\chi_3 \to Z_{\rm BL}H_3(94\%)$ $\chi_3\chi_3 \to H_3H_3(5\%)$

TABLE III. Dominant annihilation and coannihilation channels for $\sin\theta = 0.7$.

	Dominant number changing processes		
$M_{\rm DM}$ in GeV	$\Delta M = 1$	$\Delta M = 10$	$\Delta M = 100$
30	$\chi_1\chi_3 \to f\bar{f}(71\%)$ $\chi_2\chi_2 \to f\bar{f}(21\%)$	$\chi_3\chi_3 \to f\bar{f}(57\%)$ $\chi_1\chi_3 \to f\bar{f}(30\%)$ $\chi_2\chi_2 \to f\bar{f}(6\%)$	$\chi_3\chi_3 \to f\bar{f}(100\%)$
100	$\chi_1\chi_3 \to f\bar{f}(23\%)$, $\chi_3\chi_3 \to W^+W^-(17\%)$ $\chi_1\chi_3 \to W^+W^-(22\%)$, $\chi_3\chi_3 \to ZZ(6\%)$ $\chi_1\chi_3 \to ZZ(9\%)$, $\chi_1\chi_1 \to W^+W^-(8\%)$	$\chi_3\chi_3 \to W^+W^-(54\%)$ $\chi_3\chi_3 \to ZZ(20\%)$ $\chi_1\chi_3 \to W^+W^-(9\%)$	$\chi_3\chi_3 \to W^+W^-(71\%)$ $\chi_3\chi_3 \to ZZ(27\%)$
300	$\chi_1\chi_3 \to f\bar{f}(57\%)$, $\chi_1\chi_3 \to H_{1,3}H_3(9\%)$ $\chi_2\chi_2 \to f\bar{f}(21\%)$, $\chi_3\chi_3 \to H_{1,3}H_3(5\%)$ $\chi_1\chi_1 \to H_{1,3}H_3(5\%)$	$\chi_1\chi_3 \to f\bar{f}(54\%)$ $\chi_2\chi_2 \to f\bar{f}(22\%)$ $\chi_3\chi_3 \to H_{1,3}H_3(12\%)$ $\chi_1\chi_3 \to H_{1,3}H_3(10\%)$	$\chi_3\chi_3 \to H_{1,3}H_3(64\%)$ $\chi_1\chi_3 \to H_3H_3(20\%)$ $\chi_3\chi_3 \to f\bar{f}(5\%)$
1000	$\chi_1\chi_3 \to Z_{\rm BL}H_3(68\%)$ $\chi_2\chi_2 \to Z_{\rm BL}H_3(28\%)$	$\chi_1\chi_3 \to Z_{\rm BL}H_3(67\%)$ $\chi_2\chi_2 \to Z_{\rm BL}H_3(27\%)$	$\chi_1\chi_3 \to Z_{\rm BL}H_3(36\%)$ $\chi_3\chi_3 \to Z_{\rm BL}H_3(31\%)$ $\chi_2\chi_2 \to Z_{\rm BL}H_3(14\%)$ $\chi_3\chi_3 \to H_3H_3(16\%)$

However, if we consider the case of smaller $\sin\theta$ as considered for the left panel plots of Fig. 9 (i.e., $0.1 \leq \sin\theta \leq 0.2$), here DM annihilation is the most effective and hence dominantly decides the relic density and except the first term in Eq. (37), other terms are negligible. In this case, with increase in mass splitting, the effective thermal averaged cross section increases and relic density decreases. This is due to the fact that, when ΔM increases, the effective degrees of freedom $g_{\rm eff}$ decreases, which is shown in the left panel plot of Fig. 10 for a benchmark value of $M_{\rm DM}$. This, in turn, increases the $\langle\sigma v\rangle_{\rm eff}$ and hence results in decrease in the DM relic abundance.

The dominant number changing processes that can lead to the correct relic density for different DM mass is presented in Tables II, III, and IV for three different values of $\sin\theta$, i.e., $\sin\theta = 0.1, 0.7$ & 0.9 with dark fermion mass splitting $\Delta M = 1, 10$ & 100 GeV and $M_{Z_{\rm BL}} = 1000$ GeV. If DM mass is smaller than M_W, it dominantly annihilates to SM fermions through both Higgs and $Z_{\rm BL}$ exchange. As soon as kinematically allowed, DM then annihilates to W^+W^- and ZZ dominantly. Gradually with the increase in DM mass, other channels involving additional scalars also open up. Once the DM mass is beyond the $Z_{\rm BL}$ threshold, it then dominantly annihilates to $Z_{\rm BL}$ and H_3. We can see from the Table II, that for $\sin\theta = 0.1$, the dominant number

TABLE IV. Dominant annihilation and coannihilation channels for $\sin\theta = 0.9$.

	Dominant number changing processes		
$M_{\rm DM}$ in GeV	$\Delta M = 1$	$\Delta M = 10$	$\Delta M = 100$
30	$\chi_1\chi_3 \to f\bar{f}(37\%)$, $\chi_2\chi_2 \to f\bar{f}(37\%)$ $\chi_3\chi_3 \to f\bar{f}(13\%)$	$\chi_3\chi_3 \to f\bar{f}(74\%)$ $\chi_2\chi_2 \to f\bar{f}(23\%)$	$\chi_3\chi_3 \to f\bar{f}(98\%)$
100	$\chi_1\chi_3 \to f\bar{f}(12\%)$ $\chi_1\chi_1 \to W^+W^-(25\%)$ $\chi_1\chi_3 \to W^+W^-(15\%)$ $\chi_1\chi_3 \to ZZ(6\%)$ $\chi_2\chi_2 \to f\bar{f}(9\%)$ $\chi_3\chi_3 \to W^+W^-(3\%)$	$\chi_2\chi_2 \to f\bar{f}(23\%)$ $\chi_3\chi_3 \to f\bar{f}(23\%)$ $\chi_1\chi_1 \to f\bar{f}(6\%)$ $\chi_3\chi_3 \to W^+W^-(13\%)$ $\chi_3\chi_3 \to ZZ(5\%)$ $\chi_1\chi_3 \to W^+W^-(9\%)$	$\chi_3\chi_3 \to f\bar{f}(58\%)$ $\chi_3\chi_3 \to W^+W^-(30\%)$ $\chi_3\chi_3 \to ZZ(11\%)$
300	$\chi_1\chi_3 \to f\bar{f}(36\%)$ $\chi_1\chi_3 \to H_{1,3}H_3(6\%)$ $\chi_2\chi_2 \to f\bar{f}(24\%)$, $\chi_1\chi_1 \to f\bar{f}(10\%)$ $\chi_1\chi_1 \to H_{1,3}H_3(11\%)$	$\chi_1\chi_3 \to f\bar{f}(26\%)$ $\chi_2\chi_2 \to f\bar{f}(36\%)$ $\chi_3\chi_3 \to f\bar{f}(14\%)$ $\chi_1\chi_3 \to H_{1,3}H_3(10\%)$	$\chi_3\chi_3 \to H_{1,3}H_3(6\%)$ $\chi_1\chi_3 \to H_3H_3(5\%)$ $\chi_3\chi_3 \to f\bar{f}(78\%)$
1000	$\chi_1\chi_3 \to Z_{\rm BL}H_3(41\%)$ $\chi_2\chi_2 \to Z_{\rm BL}H_3(29\%)$ $\chi_3\chi_3 \to Z_{\rm BL}H_3(11\%)$ $\chi_1\chi_1 \to Z_{\rm BL}H_3(16\%)$	$\chi_1\chi_3 \to Z_{\rm BL}H_3(34\%)$ $\chi_2\chi_2 \to Z_{\rm BL}H_3(35\%)$ $\chi_3\chi_3 \to Z_{\rm BL}H_3(20\%)$ $\chi_1\chi_1 \to Z_{\rm BL}H_3(9\%)$	$\chi_1\chi_3 \to Z_{\rm BL}H_3(4\%)$ $\chi_3\chi_3 \to Z_{\rm BL}H_3(70\%)$ $\chi_2\chi_2 \to Z_{\rm BL}H_3(25\%)$

changing processes are mostly the annihilation processes irrespective of the DM mass and mass splitting, however for $\sin\theta = 0.9$ (Table IV), it is mostly the coannihilation processes that dominantly determine the relic. It is also worth noticing from these tables that the coannihilations are most effective when ΔM is smaller and with increase in ΔM, this effect gradually decreases.

To make the analysis more robust, in the left panel of Fig. 11, the correct relic density allowed parameter space has been shown in the plane of Y_{33} vs $M_{\rm DM}$ for wide range of mixing angle $\{\sin\theta = 0.1-0.3, 0.3-0.5, 0.5-0.7, 0.7-0.98\}$, indicated by different colors. To carry out this scan of parameter space, ΔM is varied randomly within 1 to 1000 GeV.

To establish the evidence of coannihilations in generating the correct relic density in this scenario, one has to compare the left and right panels of Fig. 11. In the right-panel of Fig. 11, we show the parameter space satisfying relic density constraint in the plane of Y_{33} vs $M_{\rm DM}$, considering only the annihilation processes of the DM

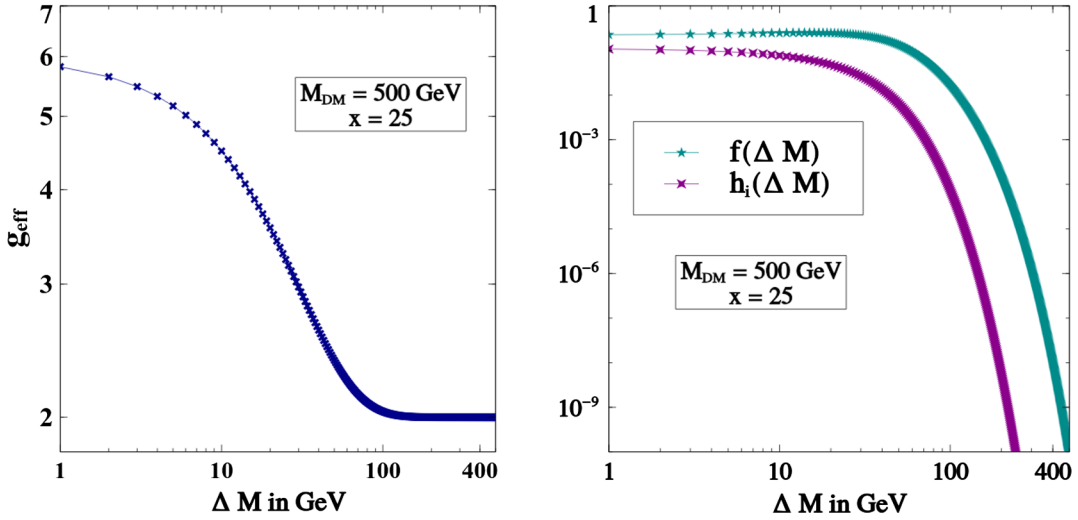

FIG. 10. Left: variation of $g_{\rm eff}$ with ΔM, Right: variation of $f(\Delta M) = \frac{2g_3g_1}{g_{\rm eff}^2}(1+\frac{\Delta M}{M_{\rm DM}})^{\frac{3}{2}}\exp(-x\frac{\Delta M}{M_{\rm DM}})$ and $h_{1,2}(\Delta M) = \frac{g_{1,2}^2}{g_{\rm eff}^2}(1+\frac{\Delta M}{M_{\rm DM}})^3\exp(-2x\frac{\Delta M}{M_{\rm DM}})$ with ΔM.

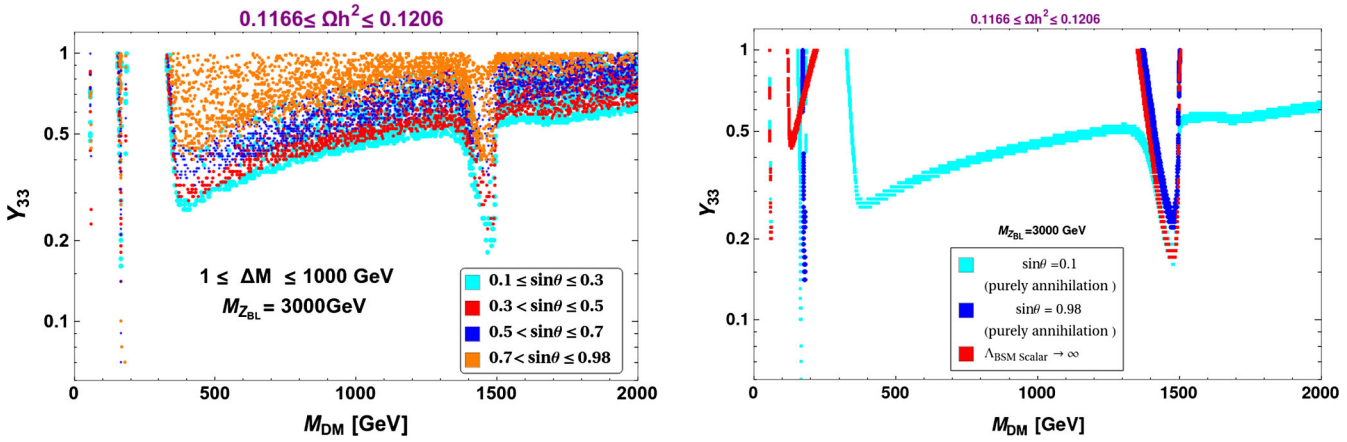

FIG. 11. Left: relic density allowed parameter space in $M_{\rm DM} - Y_{33}$ plane for different intervals of $\sin\theta$ where both annihilations and coannihilations of DM are incorporated. Right: relic density allowed parameters space in $M_{\rm DM} - Y_{33}$ plane for different $\sin\theta$ values, where only annihilation of DM is considered in different limits.

for three limiting cases: (i) small $\sin\theta$ limit, (ii) Higgs decoupling limit and (iii) large $\sin\theta$ limit.

(i) Case-I: Small $\sin\theta$ limit ($\sin\theta \to 0$)

In this case the correct relic density is obtained by setting $\sin\theta = 0.1$ as shown by the Cyan colored points in the right panel of Fig. 11. We see that apart from the resonances, the DM relic density can be satisfied for a wide range of DM mass with varying Y_{33}. This is essentially due to the presence of additional Higgses and $Z_{\rm BL}$ in the theory. The annihilation of $\chi_3\chi_3 \to H_iH_j, H_iZ_{\rm BL}$ can give rise to correct relic density beyond the resonances. As the DM mass increases, the relic density decreases which can be brought to the correct ballpark by increasing the Yukawa coupling Y_{33}. This is exactly depicted by the cyan colored points in Fig. 11.

(ii) Case-II: Higgs decoupling limit ($m_{H_i} \to \infty$)

In this case the correct relic density is obtained by setting the masses of additional Higgses to a high scale. This is shown by the red colored points in the right panel of Fig. 11. Except the Higgs masses, all other parameters are kept same as in case-I. In this case the dominant channels are $\chi_3\chi_3 \to$ SMSM mediated by SM Higgs H_1 and $Z_{\rm BL}$. We see that the relic is satisfied only in the resonance regions. This clearly demonstrates that in the small $\sin\theta$ limit (case-I) the additional Higgses only, allowing the DM mass beyond the resonance regime.

(iii) Case-III: Large $\sin\theta$ limit ($\sin\theta \to 1$)

In this case the correct relic density is obtained by setting $\sin\theta = 0.98$, while keeping all other parameters same as in case-I. We see from the right panel of Fig. 11 that the correct relic density is obtained only at the resonances as shown by the blue points. This is because in the limit: $\sin\theta \to 1$, the effective Yukawa coupling for annihilation goes to zero as shown in the left panel of Fig. 8. As a result the annihilation cross sections mentioned in case-I, i.e., $\chi_3\chi_3 \to H_iH_j, H^+H^-, H^{++}H^{--}, H_iZ_{\rm BL}$ become small, leading to an overabundance of χ_3 outside the resonances. On the other hand, near resonances the cross section increases, even if the annihilation coupling is small, and hence we get correct relic of χ_3.

Remember that in the limit $\sin\theta \to 1$, the coannihilation dominates over annihilation. See for instance, in the small ΔM limit the processes: $\chi_i\chi_j \to \bar{f}f, W^+W^-, H_iH_j, H_3Z_{\rm BL}$ as given Table IV. Now if we incorporate all the number changing processes, annihilations as well as coannihilations, as done in the left panel Fig. 11, we see that the parameter space for correct relic density is significantly enhanced. We get correct relic density of χ_3 beyond the resonance regions. This confirms that for $\sin\theta \to 1$, the coannihilation dominates. Thus from this analysis, we can infer that the coannihilations of the dark sector particles, do play a significant role in satisfying the correct relic density of the DM.

We also show the correct relic density satisfying points in the plane of ΔM and $M_{\rm DM}$ in Fig. 12, in the large $\sin\theta$ range ($\sin\theta \in [0.7, 0.98]$), where the coannihilation processes dominate over the annihilation processes. As previously discussed, the coannihilation contributions are significant if the mass-splitting ΔM is not very large. For example, in the range $\Delta M = 1$–20 GeV and DM mass in the range 1–1000 GeV, the coannihilation processes give rise a large cross section on top of annihilation and thereby creating an under abundant region. However, as ΔM increases, the coannihilation cross sections decreases. As a result, we get a correct relic density for DM mass varying in the range 1–1000 GeV. As we go from left to right, ΔM gradually decreases for a particular $\sin\theta$ to maintain the correct relic density. For DM mass beyond 1000 GeV, the annihilation cross sections decrease significantly. Therefore, we need a large coannihilation cross section

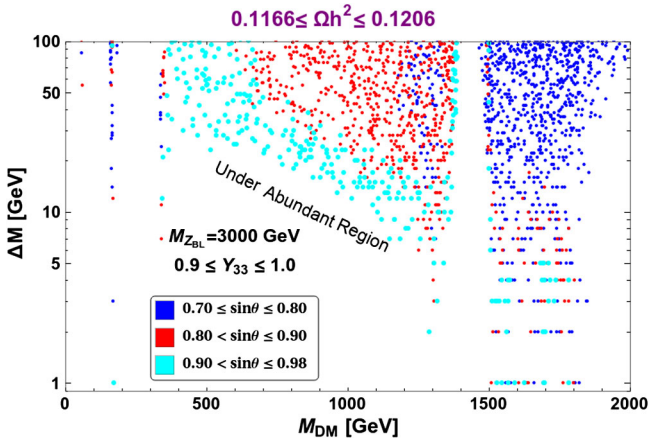

FIG. 12. Correct relic density satisfying points in the plane of ΔM and $M_{\rm DM}$ for larger values of $\sin\theta$.

to give rise the relic density in right ballpark. This can be achieved by requiring a small ΔM, typically $\Delta M < 10$ GeV. We also see from Fig. 12 that, as we move from left to right while keeping ΔM fixed (preferably at $\Delta M > 50$ GeV), large $\sin\theta$ favors a relatively small DM mass while small $\sin\theta$ prefers a large DM mass. This can be understood as follows. When $\sin\theta$ is large, $\cos\theta$ is small, which indicate less annihilation. Therefore, we need to increase the cross section by choosing a relatively smaller DM mass to bring the relic density into the observed limit. On the other hand, when $\sin\theta$ is small, $\cos\theta$ is large, which indicate larger annihilations and hence less relic. Therefore, the DM mass has to be increased in comparison to large $\sin\theta$ limit to bring the relic density into the correct ballpark.

IV. DETECTION PROSPECTS OF DM

A. Direct detection

There are various attempts to detect DM. One such major experimental procedure is the Direct detection of the DM at terrestrial laboratories through elastic scattering of the DM off nuclei. Several experiments put strict bounds on the dark matter nucleon cross section like LUX [9], PandaX-II [10,11], and XENON-1T [12,13]. In this model, the DM-nucleon scattering is possible via Higgs-mediated interaction represented by the Feynman diagram shown in Fig. 13. Here, it is worth mentioning that the DM being a Majorana fermion has only the off-diagonal (axial vector) couplings with the $Z_{\rm BL}$ boson and therefore do not contribute to spin independent direct search.

The cross section per nucleon for the spin-independent (SI) DM-nucleon interaction is given by:

$$\sigma_{SI} = \frac{1}{\pi A^2}\mu_r^2|\mathcal{M}|^2, \tag{42}$$

where A is the mass number of the target nucleus, μ_r is the reduced mass of the DM-nucleon system and $\mathcal{M}$ is the

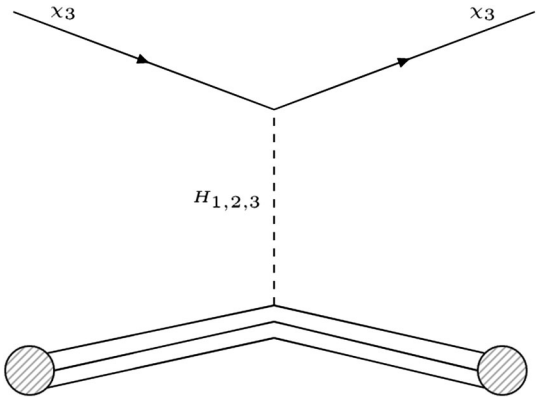

FIG. 13. Higgs-mediated DM-nucleon scattering.

amplitude for the DM-nucleon interaction, which can be written as:

$$\mathcal{M} = [Zf_p + (A-Z)f_n], \tag{43}$$

where f_p and f_n denote effective interaction strengths of DM with proton and neutron of the target used with A being mass number and Z is atomic number. The effective interaction strength can then further be decomposed in terms of interaction with partons as:

$$f^i_{p,n} = \sum_{q=u,d,s} f^{p,n}_{T_q}\alpha^i_q\frac{m_{p,n}}{m_q} + \frac{2}{27}f^{p,n}_{T_G}\sum_{Q=c,t,b}\alpha^i_Q\frac{m_{p,n}}{m_Q}, \tag{44}$$

with

$$\begin{aligned}
\alpha^1_q &= -Y_{33}\cos^2\theta\frac{m_q}{v_H}\left[\frac{(s_{12}s_{23}-c_{12}c_{23}s_{13})^2}{m^2_{H_1}}\right]\\
\alpha^2_q &= -Y_{33}\cos^2\theta\frac{m_q}{v_H}\left[\frac{(c_{12}s_{23}+c_{23}s_{12}s_{13})^2}{m^2_{H_2}}\right]\\
\alpha^3_q &= -Y_{33}\cos^2\theta\frac{m_q}{v_H}\left[\frac{(c_{13}c_{23})^2}{m^2_{H_3}}\right]
\end{aligned} \tag{45}$$

coming from DM interaction with SM via Higgs portal coupling. In Eq. (44), the different coupling strengths between DM and light quarks are given in Refs. [1,80] as $f^p_{Tu} = 0.020 \pm 0.004, f^p_{Td} = 0.026 \pm 0.005$, $f^p_{Ts} = 0.014 \pm 0.062$, $f^n_{Tu} = 0.020 \pm 0.004, f^n_{Td} = 0.036 \pm 0.005, f^n_{Ts} = 0.118 \pm 0.062$. The coupling of DM with the gluons in target nuclei is parametrized by:

$$f^{(p,n)}_{TG} = 1 - \sum_{q=u,d,s} f^{p,n}_{Tq}.$$

In the context of DM direct search, the model parameters that enter the DM-nucleon direct search cross section, are the Higgs-DM Yukawa coupling (Y_{33}) and the mixing angle ($\sin\theta$), which can be constrained by requiring that σ_{SI}

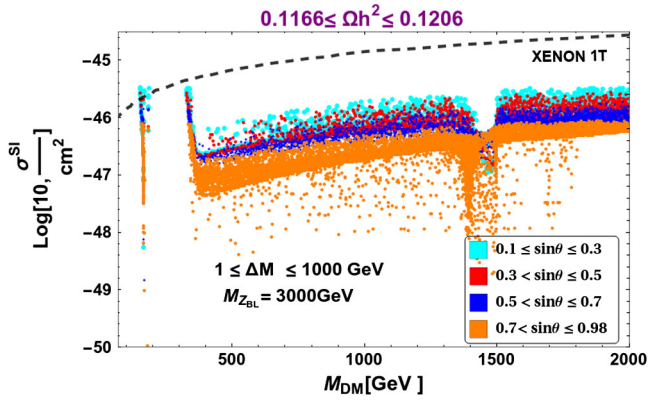

FIG. 14. Spin-independent direct detection cross section of DM with nucleon as a function of DM mass (in GeV) confronted with XENON1T data over and above relic density constraint from PLANCK.

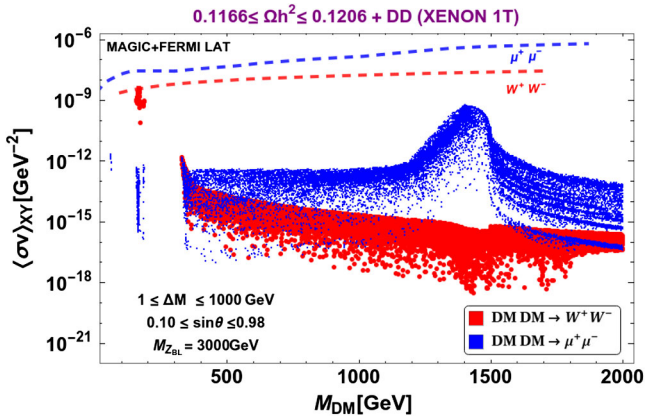

FIG. 15. $\langle\sigma v\rangle_{\chi_3\chi_3\to W^+W^-}$ and $\langle\sigma v\rangle_{\chi_3\chi_3\to\mu^+\mu^-}$ are shown as a function of $M_{\rm DM}$. Only the points satisfying both relic and DD constraints are shown. Other parameters are kept fixed as mentioned in the inset of the figure.

is less than the current DM-nucleon cross sections dictated by nonobservation of DM in current direct search data. In Fig. 14, we show the DM-nucleon cross section mediated by scalars in comparison to the latest XENON1T bound. In Fig. 14, we confronted the points satisfying relic density with the spin-independent DM-nucleon elastic scattering cross section obtained for the model as a function of DM mass. The XENON1T bound is shown by dashed black line. Thus the region below this line satisfy both relic density as well as direct detection constraint. We can see that, though for DM mass at the resonance regions, $\sin\theta$ values 0.1–0.98 can satisfy the direct detection constraint but for DM masses other than at the resonances, only larger $\sin\theta$ values ($0.7 \leq \sin\theta \leq 0.98$) are favored which is indicated by the orange points. As we have already discussed that in the larger $\sin\theta$ regime, the relic density is governed predominantly through the coannihilations of DM, so this result interestingly implies that the coannihilation effect essentially enhances the parameter space that satisfies the direct search constraints other than the resonance regions.

B. Indirect detection

Apart from direct detection experiments, DM can also be probed at different indirect detection experiments which essentially search for SM particles produced through DM annihilations. Among these final states, photon and neutrinos, being neutral and stable can reach the indirect detection experiments without getting affected much by the intermediate medium between the source and the detector. For DM in the WIMP paradigm, these photons lie in the gamma ray regime and hence can be measured at space-based telescopes like the Fermi Large Area Telescope (FermiLAT) or ground-based telescopes like MAGIC. Measuring the gamma ray flux and using the standard astrophysical inputs, one can constrain the DM annihilation into different final states like $\mu^+\mu^-, \tau^+\tau^-, W^+W^-, b\bar{b}$. Since DM cannot couple to photons directly, gamma rays can be produced from such charged final states. Using the bounds on DM annihilation to these final states from the indirect detection bounds arising from the global analysis of the Fermi-LAT and MAGIC observations of dSphs [14,15], we check for the constraints on our DM parameters.

Since there are multiple annihilation channels to different final states, the Fermi-LAT constraints on individual final states are weak for most of the cases. In Fig. 15, we show the points satisfying both relic constraint and direct search constraint confronted with the constraints from indirect detection from MAGIC + FermiLAT for annihilation of DM to W^+W^- and $\mu^+\mu^-$ which are the most stringent as compared to DM annihilation to other channels. In this model DM annihilation to W^+W^- can occur through scalar mediation as shown in right panel of Fig. 7 and DM annihilation to $\mu^+\mu^-$ can occur through scalar as well as gauge boson mediation as shown in Fig. 4. The combined bound from MAGIC and FermiLAT are shown by the dashed lines. The points below these lines are allowed by relic, direct and indirect search constraints.

C. Collider constraints on $g_{\rm BL} - M_{Z_{\rm BL}}$

Apart from constraints from relic density and direct, indirect search of DM, there exists stringent experimental constraints on the B − L gauge sector from colliders like ATLAS, CMS and LEP-II. There exists a lower bound on the ratio of new gauge boson mass to the new gauge coupling $M_{Z'}/g' \geq 7$ TeV from LEP-II data [81,82]. However the bounds from the current LHC experiments have already surpassed the LEP II limits. In particular, search for high mass dilepton resonances at ATLAS [83] and CMS [84] have put strict bounds on such additional gauge sector. In order to translate these constraints to our setup, we followed the strategy as mentioned in [85] where

the upper limit on the gauge coupling $g_{\rm BL}$ for a particular mass of gauge boson $M_{Z_{\rm BL}}$ can be derived as:

$$g_{\rm BL}^{\rm U.L.} = \sqrt{\frac{\sigma_{\rm Exp}}{\sigma_{\rm Th}/g_{\rm Th}^2}}, \tag{46}$$

where $\sigma_{\rm Exp}$ is the upper limit on the production cross section of $pp \to Z_{\rm BL} + X \to \ell^+\ell^- + X(\ell = e, \mu)$ and $\sigma_{\rm Th}$ is the cross section one obtains in their respective model for the same channel with corresponding gauge coupling $g_{\rm Th}^2$. We found that the constraint from ATLAS is more stringent than that from CMS, so we use the ATLAS ($\sqrt{s} = 13$ TeV and $\mathcal{L} = 139$ fb^{-1}) constraint to scrutinize the parameter space throughout our analysis. Here it is worth mentioning that, because of the additional decay channels of $Z_{\rm BL}$ in our model as compared to the conventional B − L scenario, the derived constraints on $g_{\rm BL} - M_{Z_{\rm BL}}$ is relatively weaker as the branching fraction ${\rm Br}(Z_{\rm BL} \to \ell^+\ell^-)$ is relatively smaller.

In Fig. 16, we show a parameter scan in the plane of $g_{\rm BL}$ vs $M_{\rm DM}$ to scrutinize our parameter space with respect to the constraints from ATLAS and LEP-II. The bounds on $g_{\rm BL}$ for a fixed $M_{Z_{\rm BL}}$ from both LEP-II and ATLAS are shown by dotted black lines for $M_{Z_{\rm BL}} = 3$ TeV. It is clear that the constraint from LEP-II is much weaker than the constraints from ATLAS. Only those points which lie below this black dotted line is allowed from all the relevant constraints (i.e., Relic + Direct Detection + Indirect Detection + ATLAS). The different colored points depict different Y_{33} values. Here it is worth mentioning that for smaller values of $M_{Z_{\rm BL}}$ around 1 TeV, the constraint from ATLAS on the corresponding $g_{\rm BL}$ is more severe, thus ruling out most of the parameter space except at the resonances and regions beyond $M_{\rm DM}$ 1 TeV corresponding to Y_{33} values larger than 0.4. However for larger values of $M_{Z_{\rm BL}}$, the corresponding constraint on $g_{\rm BL}$ from ATLAS, gradually debilitates and one can thus obtain more points satisfying all the relevant constraints.

2000 GeV ≤ $M_{Z_{\rm BL}}$ ≤ 5000 GeV:

So far whatever analysis we have done is with a fixed mass of the B − L gauge boson. We now turn to find the allowed parameter space in light of ATLAS bound on $g_{\rm BL} - M_{Z_{\rm BL}}$. The constraint on $g_{\rm BL}$ for corresponding values of $M_{Z_{\rm BL}}$ coming from the nonobservation of a new gauge boson ($Z_{\rm BL}$) at LHC from ATLAS [86] analysis is shown by the black thick dotted line in Fig. 17. This indicates that points below the line with smaller $g_{\rm BL}$ is allowed, while those above the line are ruled out. The plot shows points that satisfy relic density constraint, direct as well as indirect search constraints. Different colors indicate ranges of Y_{33} as mentioned in figure inset.

We then showcase the final parameter space in Fig. 18. In the left panel we represent the points in the plane of Y_{33} vs $M_{\rm DM}$ after imposing the bounds from correct relic density of DM, direct and indirect detection of DM and search for B − L gauge boson at ATLAS. Clearly there is enough parameter space beyond the resonance regions that is allowed from all the relevant constraints. Also the points with larger $\sin\theta$ which represents the dominant coannihilation of dark sector fermions play a significant role in giving correct relic density as well as satisfying all other phenomenological and experimental constraints.

To specifically depict the parameter space where the coannihilations do play a significant role, we show the parameter space with larger dark fermion mixing angle ($\sin\theta \in [0.7, 1]$), in the plane of ΔM vs $M_{\rm DM}$. Clearly, for $\sin\theta \to 1$ (blue colored points), as we increase the DM mass, $\langle\sigma v\rangle_{\rm eff}$ decreases which can be compensated by the help of more coannihilation contributions that can be achieved by decreasing mass-splittings.

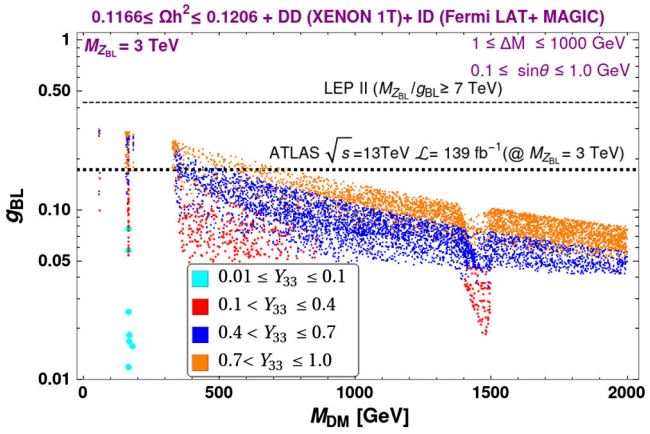

FIG. 16. Parameter space satisfying relic, direct detection, and indirect detection constraints are shown in $g_{\rm BL}$ vs $M_{\rm DM}$ plot. ATLAS and LEP-II bounds are shown for $M_{Z_{\rm BL}} = 3$ TeV by the black dotted lines.

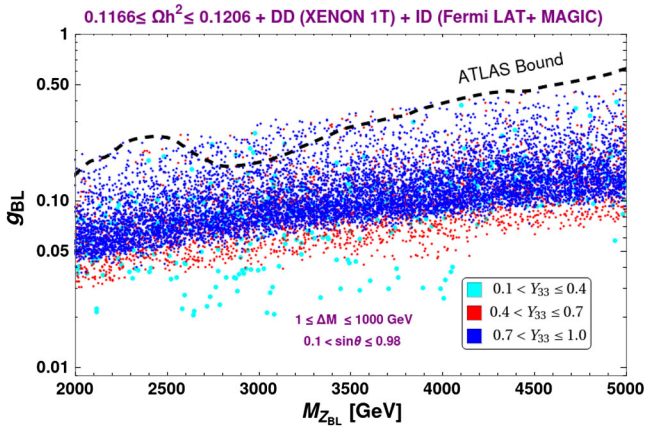

FIG. 17. Relic, direct detection and indirect detection satisfied points are shown in the plane of $g_{\rm BL} - M_{Z_{\rm BL}}$ plane with different range of Y_{33}. The thick black dotted line shows the ATLAS bound on $g_{\rm BL} vs M_{Z_{\rm BL}}$ plane from nonobservation of $Z_{\rm BL}$ at colliders.

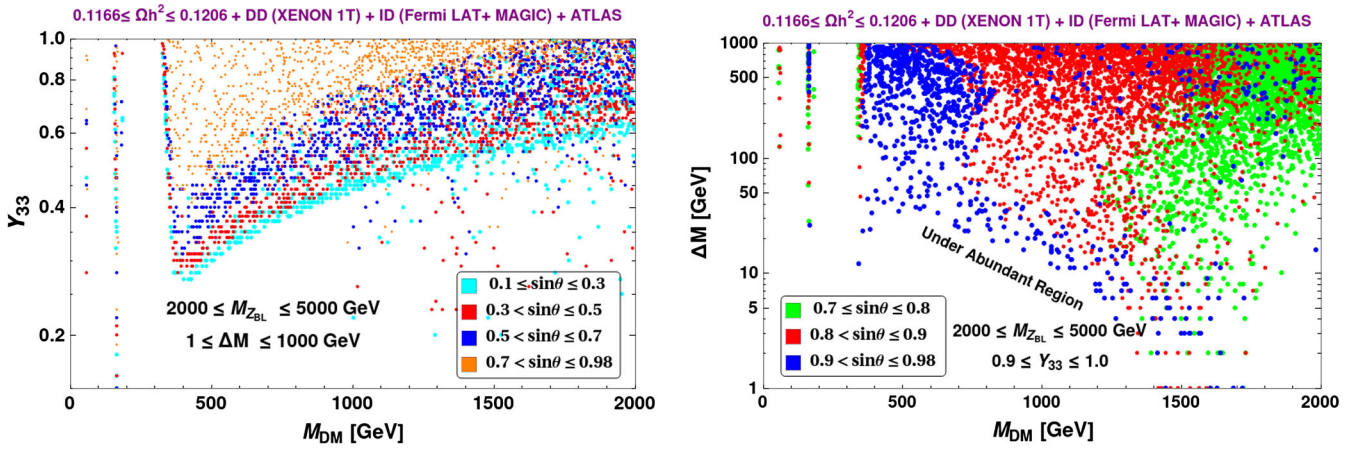

FIG. 18. Left: parameter space satisfying relic density, direct and indirect detection bound as well as $g_{\rm BL} - M_{Z_{\rm BL}}$ constraint from ATLAS is shown in the plane of $Y_{33} vs M_{\rm DM}$. Right: parameter space satisfying all constraints in the plane of ΔM and $M_{\rm DM}$ for larger values of $\sin\theta$.

V. COLLIDER SIGNATURE OF DOUBLY CHARGED SCALAR IN PRESENCE OF $Z_{\rm BL}$

The light doubly charged scalar in this model offers novel multilepton signatures with missing energy and jets. It is worthy of mentioning here that the dark sector which contains the gauge singlet Majorana fermions do not have any promising collider signatures as the mono-X type signal processes arising out of initial state radiation are extremely suppressed. The doubly charged scalar, $H^{\pm\pm}$ which is also charged under $U(1)_{\rm B-L}$ can be produced at Large Hadron Collider (LHC) via Higgs ($H_{1,2,3}$) and gauge bosons ($\gamma, Z, Z_{\rm BL}$) mediations. Further decay of $H^{\pm\pm}$ to $W^{\pm}W^{\pm}$ pair (assumed $m_{H^{\pm\pm}} \geq 2m_W$) with almost 100% branching ratio for $v_\xi \sim 2.951$ GeV yields $W^+W^+W^-W^-$ final state. As a result the four W final state offers: $4\ell + \not{E}_T$ and $m\ell + nj + \not{E}_T$ signatures at collider. For details of branching fraction and partial decay widths of H^{++} with v_ξ, please see Appendix B. Although these types of signatures have been studied in the context of type-II seesaw model, the triplet scalar ξ considered in this model also have $U(1)_{\rm B-L}$ charge on top SM gauge charges and that makes this model different from the usual type-II seesaw scenario. In this section we will briefly highlight the effect of additional gauge boson $Z_{\rm BL}$ on the pair production cross section of doubly charged scalar. The corresponding Feynman diagram of this type process is shown in Fig. 19.

The pair production cross section of doubly charged scalar, $H^{++}H^{--}$ as function of mass, $m_{H^{\pm\pm}}$ for fixed value of $M_{Z_{\rm BL}} = 4.5$ TeV with $\sqrt{s} = 13$ TeV is shown in Fig. 20. The production cross sections are computed in MicrOmegas using the NNPDF23 parton distributions. The black solid line corresponds to the case where $U(1)_{\rm B-L}$ gauge boson, $Z_{\rm BL}$ is absent and the scenario resembles the usual type-II seesaw scenario. And in that case the $H^{++}H^{--}$ pair can be produced via SM Higgs and SM gauge boson (γ, Z) mediated Drell-Yan processes. However in a gauged B − L scenario, the presence of the additional gauge boson $Z_{\rm BL}$ can affect this pair production cross section of $H^{++}H^{--}$. The effects of $U(1)_{\rm B-L}$ gauge boson on top of SM gauge bosons are shown by dotted lines in the Fig. 20 for two different values of gauge couplings: $g_{\rm BL} = 0.33$ (purple line) and 0.44 (blue line). It is important to note here that the above values of the $g_{\rm BL}$ can be obtained using the Eq. (31) keeping the other parameters fixed as mentioned in the inset of the figure. For illustration purpose we considered two moderate values of $g_{\rm BL}$: 0.33 (purple dashed line) and 0.44 (blue dashed line) which are in agreement with the current ATLAS bound $g_{\rm BL} \leq 0.47$ for $M_{Z_{\rm BL}} = 4.5$ TeV. It is noticeable from the graph that the presence of $Z_{\rm BL}$ enhances the production cross section toward the heavy mass region of doubly charged scalar with moderate value of $g_{\rm BL}$ compared to the case without $U(1)_{\rm B-L}$ augmentation. It is because of the on-shell decay of $Z_{\rm BL}$ to $H^{++}H^{--}$ pair as $M_{Z_{\rm BL}} > 2m_{H^{\pm\pm}}$ and there is a

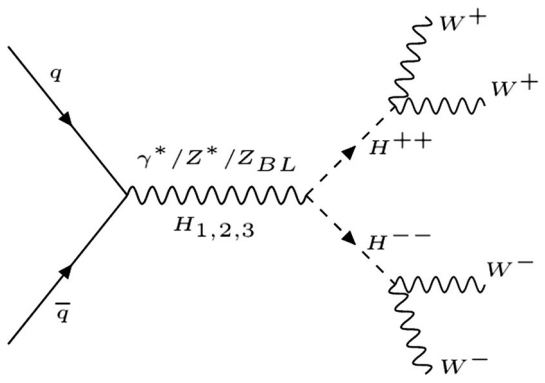

FIG. 19. Feynman diagram for pair production of doubly charged scalar at LHC via Higgs ($H_{1,2,3}$) and gauge bosons ($\gamma, Z, Z_{\rm BL}$) mediations.

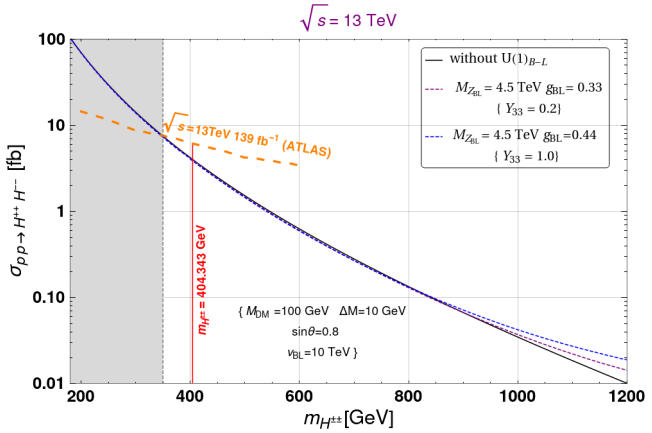

FIG. 20. Production cross section for $pp \to H^{++}H^{--}$ as a function of doubly charged scalar mass $m_{H^{\pm\pm}}$ considering Br $(H^{\pm\pm} \to W^{\pm}W^{\pm}) \sim 100\%$ at $\sqrt{s} = 14$ TeV. The black solid line corresponds to the usual type-II seesaw scenario where $Z_{\rm BL}$ gauge mediated diagrams are absent. The effects of $Z_{\rm BL}$ on the production cross section are shown dashed in dashed lines: purple line ($M_{Z_{\rm BL}} = 4.5$ TeV, $g_{\rm BL} = 0.33$) and blue line ($M_{Z_{\rm BL}} = 4.5$ TeV, $g_{\rm BL} = 0.44$). Other parameters are fixed as mentioned inset of the figure. The shaded region is excluded from ATLAS data on doubly charged scalar mass, $m_{H^{\pm\pm}}$ for $\sqrt{s} =$ 13 TeV and luminosity 139 fb^{-1}.

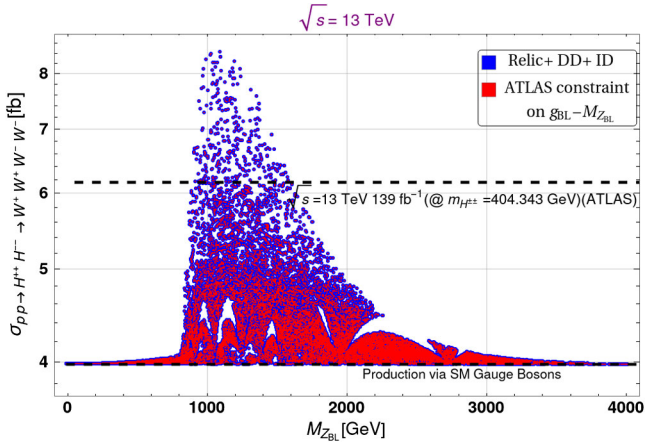

FIG. 21. The model parameters are projected against the production cross section of doubly charged scalar ($H^{\pm\pm}$) as a function of B − L gauge boson mass $M_{Z_{\rm BL}}$. The blue points are satisfying the Relic + Direct Detection + Indirect Detection constraints. Red points are consistent with the ATLAS constraint on $g_{\rm BL} - M_{Z_{\rm BL}}$.

constructive interference between $Z_{\rm BL}$ and the SM gauge bosons. The orange dashed line shows the observed and expected upper limit on $H^{++}H^{--}$ pair production cross section as a function of doubly charged scalar mass $m_{H^{\pm\pm}}$ at 95% CL which is obtained from the combination of multileptons with jets plus missing energy search at ATLAS with $\sqrt{s} = 13$ TeV and integrated luminosity, $\mathcal{L} = 139$ fb^{-1} [87]. This upper limit of production cross section excludes the region of doubly charged triplet mass,$m_{H^{\pm\pm}} \leq 350$ GeV as shown by the shaded region in Fig. 20.

In Fig. 21, we projected the points satisfying all the relevant constraints against the doubly charged scalar ($H^{\pm\pm}$) production cross section as a function of B − L gauge boson mass $M_{Z_{\rm BL}}$ with $\sqrt{s} = 13$ TeV for a benchmark value of $m_{H^{\pm\pm}} = 404.343$ GeV. The black dashed line shows the upper limit on the production cross section from ATLAS [87]. The blue points show the parameters that satisfy all the relevant constraints like correct relic density, direct and indirect search of DM and the red points are obtained after imposing the constraints from ATLAS on $g_{\rm BL}$ and $M_{Z_{\rm BL}}$. We can see that in presence of the B − L gauge boson, the production cross section $\sigma_{pp\to H^{++}H^{--}}$ can get a distinctive enhancement as compared to the case where production of $H^{\pm\pm}$ happens through SM gauge bosons (γ^*, Z^*) mediation only which is shown as the dashed black line at the bottom for easy comparison. As is clear from the Fig. 21, near the resonance (i.e., $M_{Z_{\rm BL}} = 2m_{H^{++}}$), we see maximum enhancement in the production cross section which is again constrained from the $4W$ final state at ATLAS and the points above the orange dotted line are ruled out.

Similar perceptible signal can be seen at the collider if we consider the doubly charged scalar mass in the TeV scale too, requiring a higher $M_{Z_{\rm BL}}$ (> 2 TeV) for the resonance enhancement to happen. Thus to demonstrate this fact, we considered the doubly charged scalar mass $m_{H^{\pm\pm}} = 1$ TeV. In Fig. 22, we show the production cross section of doubly charged scalar ($H^{\pm\pm}$) as a function of $M_{Z_{\rm BL}}$ considering the gauge coupling within the interval $0.001 \leq g_{\rm BL} \leq 0.50$ with $\sqrt{s} = 14$ TeV shown by the orange points. Though the constraints from the current LHC experiments have already surpassed the LEP II limits

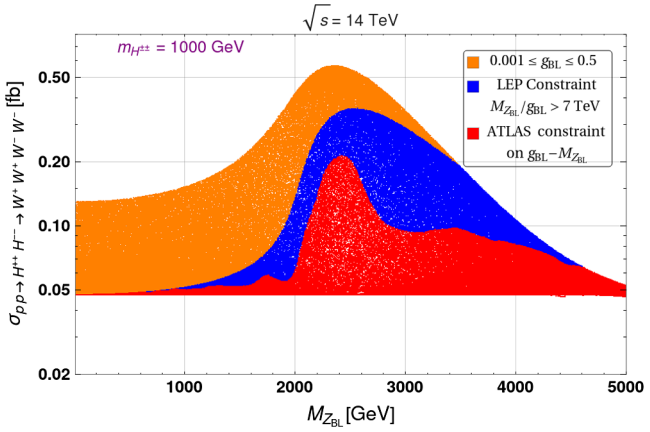

FIG. 22. The production cross section of doubly charged scalar ($H^{\pm\pm}$) as a function of $M_{Z_{\rm BL}}$. The orange points correspond to gauge coupling:$0.001 \leq g_{\rm BL} \leq 0.50$. The blue points are allowed from LEP exclusion bound. Red points are consistent with ATLAS constraint on $g_{\rm BL} - M_{Z_{\rm BL}}$.

on $g_{\rm BL} - M_{Z_{\rm BL}}$, for comparison we show the blue points in the plot which depicts the maximum increase in $\sigma_{pp\to H^{++}H^{--}}$ when the constraint from LEP on $g_{\rm BL} - M_{Z_{\rm BL}}$ is incorporated into the calculation. However, even after imposing the most stringent constraint from ATLAS on $g_{\rm BL} - M_{Z_{\rm BL}}$, we observe that there is a noteworthy enhancement in the production of $H^{\pm\pm}$ as compared to the value predicted by SM. The production cross section $\sigma_{pp\to H^{++}H^{--}}$ increases by almost 300% (0.21 fb in presence of $Z_{\rm BL}$ as compared to 0.047 fb predicted by SM) at the resonance. Apart from resonance also, there is significant enhancement for other masses of $Z_{\rm BL}$; for example, we see an enhancement by almost 90% (∼0.09 fb in presence of $Z_{\rm BL}$ as compared to 0.047 fb predicted by SM) for $M_{Z_{\rm BL}}$ around 3.5 TeV. This feature is evident from the red points in Fig. 22. This is the crucial evidence of the scenario considered here that can be probed by the near and future colliders and hence the feasibility of this model can be verified.

This also establishes an interesting connection between the dark sector and the generation of neutrino mass via the modified type-II seesaw in a gauged B − L setup that we discussed.

VI. SUMMARY AND CONCLUSIONS

In this paper, we have studied a very well motivated gauge extension of the standard model by augmenting the SM gauge group with a $U(1)_{\rm B-L}$ symmetry, which happens to be an accidental symmetry of SM, to simultaneously address nonzero masses of light neutrinos as well as a phenomenologically viable dark matter component of the universe. We minimally extend the fermion particle content of the model by adding three exotic right chiral fermions χ_{i_R} with B − L charges $-4, -4$ and $+5$ in order to cancel the gauge and gravitational anomalies that arise when one gauges the B − L symmetry. The stability of these fermions is owed to the remnant $\mathcal{Z}_2$ symmetry after the $U(1)_{\rm B-L}$ breaking which distinguishes the added fermions from the SM as $\chi_{i_R}(i = e, \mu, \tau)$ are odd under $\mathcal{Z}_2$ while all other particles are even. Thus the dark matter emerges as the lightest Majorana fermion from the mixture of these exotic fermions.

A very interesting and important aspect of the model is the correlation between dark sector and neutrino mass generation. The neutrino mass is explained through a modified type-II seesaw at TeV scale by introducing two $SU(2)_L$ triplet scalars Δ and ξ. Δ is super heavy and does not have a coupling with the lepton and hence cannot generate the neutrino mass even after acquiring an induced vev after the EW symmetry breaking. Thus the neutrino mass is essentially generated through the ξLL coupling as given in Eq. (10). In the limit $v_{\rm BL} \to 0$, which essentially means vanishing mixing between Δ and ξ, the neutrino mass also vanishes. Also Eqs. (2), (24), and (27) implies that the interactions between χ_{τ_R} and χ_{e_R}, χ_{μ_R} are established through the scalar $\Phi_{\rm BL}$. In the limit of $\langle\Phi_{\rm BL}\rangle \to 0$, which essentially implies $\sin\theta \to 0$, the DM candidate χ_3 decouples from the heavier dark particles χ_1 and χ_2. In this limit there will be no coannihilations among the dark sector particles. Thus only if $\langle\Phi_{\rm BL}\rangle \neq 0$, we get nonzero masses of light neutrinos as well as it switches on the coannihilations of DM and hence enlarges the parameter space satisfying all relevant constraints.

We studied the model parameter space by taking into account all annihilation and coannihilation channels for DM mass ranging from 1 GeV to 2 TeV. We confronted our results with recent data from PLANCK and XENON1T to obtain the parameter space satisfying relic density as well as direct detection constraints. The DM being Majorana in nature, it escapes from the gauge boson mediated direct detection constraint. We also checked for the constraints on our model parameters from the indirect search of DM using the recent data from Fermi-LAT and MAGIC which we found to be relatively weaker than other constraints. We also imposed the constraint on $g_{\rm BL} - M_{Z_{\rm BL}}$ from current LHC data to obtain the final parameter space allowed from all constraints including correct relic, direct and indirect detection of DM as well as the constraints from colliders on the B − L gauge boson and the corresponding coupling.

We also studied the detection prospects of the doubly charged scalar triplet which can have novel signatures at the colliders with multileptons along with missing energy and jets. We showed how in the presence of the B − L gauge boson $Z_{\rm BL}$, the pair production cross section of $H^{++}H^{--}$ can get enhanced and also depicted how the dark parameters satisfying all the relevant constraints can affect the production of this doubly charged scalar.

ACKNOWLEDGMENTS

S. M. would like to acknowledge Alexander Belyaev and Alexander Pukhov for useful discussions. S. M. also thanks A. Das and P. S. B. Dev for useful discussions. P. G. would like to acknowledge the support from DAE, India for the Regional Centre for Accelerator based Particle Physics (RECAPP), Harish Chandra Research Institute. N. S. acknowledges the support from Department of Atomic Energy (DAE)- Board of Research in Nuclear Sciences (BRNS), Government of India (Ref. Number: 58/14/15/2021-BRNS/37220).

APPENDIX A: ANOMALY CANCELLATION

In any chiral gauge theory the anomaly coefficient is given by [88]:

$$\mathcal{A} = \mathrm{Tr}[T_a[T_b, T_c]_+]_R - \mathrm{Tr}[Ta[T_b, T_c]_+]_L, \quad \text{(A1)}$$

where T denotes the generators of the gauge group and R, L represent the interactions of right and left chiral fermions with the gauge bosons.

Gauging of $U(1)_{B-L}$ symmetry within the SM lead to the following triangle anomalies:

$$\mathcal{A}_1[U(1)^3_{B-L}] = 3$$
$$\mathcal{A}_2[(\text{Gravity})^2 \times U(1)_{B-L}] = 3. \quad \text{(A2)}$$

The natural choice to make the gauged $B-L$ model anomaly free is by introducing three right handed neutrinos, each of having $B-L$ charge -1 such that they result in $\mathcal{A}_1[U(1)^3_{B-L}] = -3$ and $\mathcal{A}_2[(\text{Gravity})^2 \times U(1)_{B-L}] = -3$ which lead to cancellation of above mentioned gauge anomalies.

However we can have alternative ways of constructing anomaly free versions of $U(1)_{B-L}$ extension of the SM. In particular, three right chiral fermions with exotic $B-L$ charges -4, -4, $+5$ can also give rise to vanishing $B-L$ anomalies.

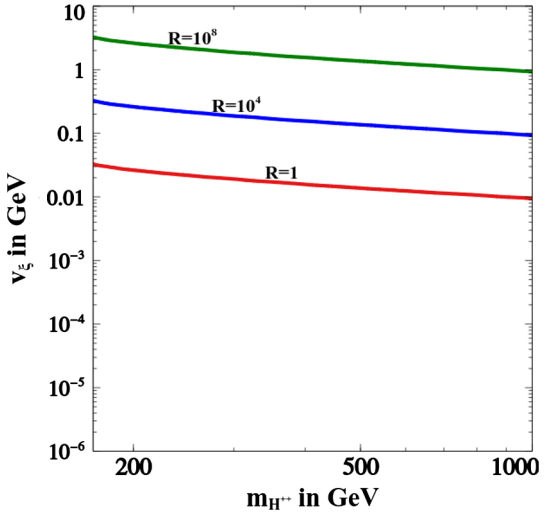

FIG. 23. The contour for R in the plane of v_ξ vs $m_{H^{++}}$.

$$\mathcal{A}_1[U(1)^3_{B-L}] = \mathcal{A}_1^{\text{SM}}[U(1)^3_{B-L}] + \mathcal{A}_1^{\text{New}}[U(1)^3_{B-L}] = 3 + [(-4)^3 + (-4)^3 + (5)^3] = 0$$
$$\mathcal{A}_2[(\text{Gravity})^2 \times U(1)_{B-L}] = \mathcal{A}_2^{\text{SM}}[(\text{Gravity})^2 \times U(1)_{B-L}] + \mathcal{A}_2^{\text{New}}[(\text{Gravity})^2 \times U(1)_{B-L}]$$
$$= 3 + [(-4) + (-4) + (5)] = 0. \quad \text{(A3)}$$

APPENDIX B: DECAY OF DOUBLY CHARGED SCALAR

The partial decay widths of the doubly charged scalar (H^{++}) are given as:

$$\Gamma(H^{++} \to l^+_\alpha l^+_\beta) = \frac{m_{H^{++}}}{4\pi v_\xi^2(1+\delta_{\alpha\beta})}|(M_\nu)_{\alpha\beta}|^2 \quad \text{(B1)}$$

and

$$\Gamma(H^{++} \to W^+W^+) = g^4 v_\xi^2 m^3_{H^{++}}\left[1-4\left(\frac{m_W}{m_{H^{++}}}\right)^2\right]^{\frac{1}{2}} \times \left[1-4\left(\frac{m_W}{m_{H^{++}}}\right)^2 + \left(\frac{m_W}{m_{H^{++}}}\right)^4\right]. \quad \text{(B2)}$$

This can be well analyzed by plotting contours of the ratio

$$R = \frac{\Gamma(H^{++} \to W^+W^+)}{\Gamma(H^{++} \to l^+_\alpha l^+_\beta)} \quad \text{(B3)}$$

in the plane of $m_{H^{++}}$ vs v_ξ as shown in the Fig. 23. It can be easily inferred from Fig. 23 that if v_ξ is a few hundred MeV or more, then H^{++} dominantly decays to W^+W^+.

[1] G. Bertone, D. Hooper, and J. Silk, Particle dark matter: Evidence, candidates and constraints, Phys. Rep. **405**, 279 (2005).
[2] F. Zwicky, Die Rotverschiebung von extragalaktischen Nebeln, Helv. Phys. Acta **6**, 110 (1933); Gen. Relativ. Gravit. **41**, 207 (2009).
[3] V. C. Rubin and W. K. Ford, Jr., Rotation of the andromeda nebula from a spectroscopic survey of emission regions, Astrophys. J. **159**, 379 (1970).
[4] D. Clowe, M. Bradac, A. H. Gonzalez, M. Markevitch, S. W. Randall, C. Jones, and D. Zaritsky, A direct empirical proof of the existence of dark matter, Astrophys. J. **648**, L109 (2006).
[5] G. Hinshaw *et al.* (WMAP Collaboration), Nine-year Wilkinson Microwave Anisotropy Probe (WMAP) observations: Cosmological parameter results, Astrophys. J. Suppl. Ser. **208**, 19 (2013).

[6] N. Aghanim *et al.* (Planck Collaboration), Planck 2018 results. VI. Cosmological parameters, Astron. Astrophys. **641**, A6 (2020).
[7] E. W. Kolb and M. S. Turner, The early universe, Front. Phys. **69**, 1 (1990).
[8] G. Arcadi, M. Dutra, P. Ghosh, M. Lindner, Y. Mambrini, M. Pierre, S. Profumo, and F. S. Queiroz, The waning of the WIMP? A review of models, searches, and constraints, Eur. Phys. J. C **78**, 203 (2018).
[9] D. S. Akerib *et al.* (LUX Collaboration), Results from a Search for Dark Matter in the Complete LUX Exposure, Phys. Rev. Lett. **118**, 021303 (2017).
[10] A. Tan *et al.* (PandaX-II Collaboration), Dark Matter Results from First 98.7 Days of Data from the PandaX-II Experiment, Phys. Rev. Lett. **117**, 121303 (2016).
[11] X. Cui *et al.* (PandaX-II Collaboration), Dark Matter Results From 54-Ton-Day Exposure of PandaX-II Experiment, Phys. Rev. Lett. **119**, 181302 (2017).
[12] E. Aprile *et al.* (XENON Collaboration), First Dark Matter Search Results from the XENON1T Experiment, Phys. Rev. Lett. **119**, 181301 (2017).
[13] E. Aprile *et al.* (XENON Collaboration), Dark Matter Search Results from a One Ton-Year Exposure of XENON1T, Phys. Rev. Lett. **121**, 111302 (2018).
[14] M. Ackermann *et al.* (Fermi-LAT Collaboration), Searching for Dark Matter Annihilation from Milky Way Dwarf Spheroidal Galaxies with Six Years of Fermi Large Area Telescope Data, Phys. Rev. Lett. **115**, 231301 (2015).
[15] M. L. Ahnen *et al.* (Fermi-LAT, MAGIC Collaborations), Limits to dark matter annihilation cross-section from a combined analysis of MAGIC and Fermi-LAT observations of dwarf satellite galaxies, J. Cosmol. Astropart. Phys. 02 (2016) 039.
[16] Y. Fukuda *et al.* (Super-Kamiokande Collaboration), Evidence for Oscillation of Atmospheric Neutrinos, Phys. Rev. Lett. **81**, 1562 (1998).
[17] Q. R. Ahmad *et al.* (SNO Collaboration), Measurement of the Rate of $\nu_e + d \to p + p + e^-$ Interactions Produced by ^{8}B Solar Neutrinos at the Sudbury Neutrino Observatory, Phys. Rev. Lett. **87**, 071301 (2001).
[18] Y. Abe *et al.* (Double Chooz Collaboration), Indication of Reactor $\bar{\nu}_e$ Disappearance in the Double Chooz Experiment, Phys. Rev. Lett. **108**, 131801 (2012).
[19] F. P. An *et al.* (Daya Bay Collaboration), Observation of Electron-Antineutrino Disappearance at Daya Bay, Phys. Rev. Lett. **108**, 171803 (2012).
[20] J. K. Ahn *et al.* (RENO Collaboration), Observation of Reactor Electron Antineutrino Disappearance in the RENO Experiment, Phys. Rev. Lett. **108**, 191802 (2012).
[21] M. Tanabashi *et al.* (Particle Data Group Collaboration), Review of particle physics, Phys. Rev. D **98**, 030001 (2018).
[22] S. Vagnozzi, E. Giusarma, O. Mena, K. Freese, M. Gerbino, S. Ho, and M. Lattanzi, Unveiling ν secrets with cosmological data: Neutrino masses and mass hierarchy, Phys. Rev. D **96**, 123503 (2017).
[23] E. Giusarma, M. Gerbino, O. Mena, S. Vagnozzi, S. Ho, and K. Freese, Improvement of cosmological neutrino mass bounds, Phys. Rev. D **94**, 083522 (2016).
[24] E. Giusarma, S. Vagnozzi, S. Ho, S. Ferraro, K. Freese, R. Kamen-Rubio, and K.-B. Luk, Scale-dependent galaxy bias, CMB lensing-galaxy cross-correlation, and neutrino masses, Phys. Rev. D **98**, 123526 (2018).
[25] I. Esteban, M. C. Gonzalez-Garcia, A. Hernandez-Cabezudo, M. Maltoni, and T. Schwetz, Global analysis of three-flavour neutrino oscillations: Synergies and tensions in the determination of $\theta_2 3, \delta_C P$, and the mass ordering, J. High Energy Phys. 01 (2019) 106.
[26] P. Minkowski, $\mu \to e\gamma$ at a rate of one out of 10^9 muon decays?, Phys. Lett. **67B**, 421 (1977).
[27] M. Gell-Mann, P. Ramond, and R. Slansky, Complex spinors and unified theories, Conf. Proc. **C790927**, 315 (1979).
[28] R. N. Mohapatra and G. Senjanovic, Neutrino Mass and Spontaneous Parity Violation, Phys. Rev. Lett. **44**, 912 (1980).
[29] J. Schechter and J. W. F. Valle, Neutrino masses in $SU(2) \times U(1)$ theories, Phys. Rev. D **22**, 2227 (1980).
[30] A. Davidson and K. C. Wali, Universal Seesaw Mechanism?, Phys. Rev. Lett. **59**, 393 (1987).
[31] R. N. Mohapatra and G. Senjanovic, Neutrino masses and mixings in gauge models with spontaneous parity violation, Phys. Rev. D **23**, 165 (1981).
[32] G. Lazarides, Q. Shafi, and C. Wetterich, Proton lifetime and fermion masses in an SO(10) model, Nucl. Phys. **B181**, 287 (1981).
[33] J. Schechter and J. W. F. Valle, Neutrino decay and spontaneous violation of lepton number, Phys. Rev. D **25**, 774 (1982).
[34] C. Wetterich, Neutrino masses and the scale of $B - L$ violation, Nucl. Phys. **B187**, 343 (1981).
[35] B. Brahmachari and R. N. Mohapatra, Unified explanation of the solar and atmospheric neutrino puzzles in a minimal supersymmetric SO(10) model, Phys. Rev. D **58**, 015001 (1998).
[36] R. Foot, H. Lew, X. G. He, and G. C. Joshi, Seesaw neutrino masses induced by a triplet of leptons, Z. Phys. C **44**, 441 (1989).
[37] S. Weinberg, Baryon and Lepton Nonconserving Processes, Phys. Rev. Lett. **43**, 1566 (1979).
[38] E. Ma, Pathways to Naturally Small Neutrino Masses, Phys. Rev. Lett. **81**, 1171 (1998).
[39] J. McDonald, N. Sahu, and U. Sarkar, Type-II seesaw at collider, lepton asymmetry and singlet scalar dark matter, J. Cosmol. Astropart. Phys. 04 (2008) 037.
[40] P.-H. Gu, H.-J. He, U. Sarkar, and X.-m. Zhang, Double type-II seesaw, baryon asymmetry and dark matter for cosmic $e^{\pm}$ excesses, Phys. Rev. D **80**, 053004 (2009).
[41] S. K. Majee and N. Sahu, Dilepton signal of a type-II seesaw at CERN LHC: Reveals a TeV scale $B - L$ symmetry, Phys. Rev. D **82**, 053007 (2010).
[42] K. Huitu, J. Maalampi, A. Pietila, and M. Raidal, Doubly charged Higgs at LHC, Nucl. Phys. **B487**, 27 (1997).
[43] E. J. Chun, K. Y. Lee, and S. C. Park, Testing Higgs triplet model and neutrino mass patterns, Phys. Lett. B **566**, 142 (2003).
[44] P. Fileviez Perez, T. Han, G.-y. Huang, T. Li, and K. Wang, Neutrino masses and the CERN LHC: Testing type II seesaw, Phys. Rev. D **78**, 015018 (2008).

[45] R. Padhan, D. Das, M. Mitra, and A. Kumar Nayak, Probing doubly and singly charged Higgs bosons at the pp collider HE-LHC, Phys. Rev. D **101**, 075050 (2020).
[46] P. S. Bhupal Dev and Y. Zhang, Displaced vertex signatures of doubly charged scalars in the type-II seesaw and its left-right extensions, J. High Energy Phys. 10 (2018) 199.
[47] B. Barman, S. Bhattacharya, P. Ghosh, S. Kadam, and N. Sahu, Fermion dark matter with scalar triplet at direct and collider searches, Phys. Rev. D **100**, 015027 (2019).
[48] S. Bhattacharya, P. Ghosh, N. Sahoo, and N. Sahu, A mini-review on vector-like leptonic dark matter, neutrino mass and collider signatures, Front. Phys. **7**, 80 (2019).
[49] J. G. Rodrigues, A. C. O. Santos, J. G. Ferreira, Jr., and C. A. de S. Pires, Neutrino masses, cosmological inflation and dark matter in a variant $U(1)_{B-L}$ model with type II seesaw mechanism, Chin. Phys. C **45**, 025110 (2021).
[50] D. Borah, D. Nanda, N. Narendra, and N. Sahu, Right-handed neutrino dark matter with radiative neutrino mass in gauged $B-L$ model, Nucl. Phys. **B950**, 114841 (2020).
[51] J. C. Montero and V. Pleitez, Gauging U(1) symmetries and the number of right-handed neutrinos, Phys. Lett. B **675**, 64 (2009).
[52] E. Ma and R. Srivastava, Dirac or inverse seesaw neutrino masses with $B-L$ gauge symmetry and S_3 flavor symmetry, Phys. Lett. B **741**, 217 (2015).
[53] B. L. Snchez-Vega and E. R. Schmitz, Fermionic dark matter and neutrino masses in a $B-L$ model, Phys. Rev. D **92**, 053007 (2015).
[54] S. Singirala, R. Mohanta, S. Patra, and S. Rao, Majorana dark matter in a new $B-L$ model, J. Cosmol. Astropart. Phys. 11 (2018) 026.
[55] N. Okada, S. Okada, and D. Raut, A natural Z'-portal Majorana dark matter in alternative U(1) extended Standard Model, Phys. Rev. D **100**, 035022 (2019).
[56] K. Asai, K. Nakayama, and S.-Y. Tseng, Alternative minimal $U(1)_{B-L}$, Phys. Lett. B **814**, 136106 (2021).
[57] S. Mahapatra, N. Narendra, and N. Sahu, Verifiable type-II seesaw and dark matter in a gauged $U(1)_{B-L}$ model, arXiv:2002.07000.
[58] A. Davidson, $B-L$ as the fourth color within an $\mathrm{SU}(2)_L \times \mathrm{U}(1)_R \times \mathrm{U}(1)$ model, Phys. Rev. D **20**, 776 (1979).
[59] R. N. Mohapatra and R. E. Marshak, Local $B-L$ Symmetry of Electroweak Interactions, Majorana Neutrinos and Neutron Oscillations, Phys. Rev. Lett. **44**, 1316 (1980); **44**, 1643(E) (1980).
[60] R. E. Marshak and R. N. Mohapatra, Quark-lepton symmetry and $B-L$ as the U(1) generator of the electroweak symmetry group, Phys. Lett. **91B**, 222 (1980).
[61] A. Masiero, J. F. Nieves, and T. Yanagida, $B-L$ violating proton decay and late cosmological baryon production, Phys. Lett. **116B**, 11 (1982).
[62] R. N. Mohapatra and G. Senjanovic, Spontaneous breaking of global $B-L$ symmetry and matter—antimatter oscillations in grand unified theories, Phys. Rev. D **27**, 254 (1983).
[63] W. Buchmuller, C. Greub, and P. Minkowski, Neutrino masses, neutral vector bosons and the scale of $B-L$ breaking, Phys. Lett. B **267**, 395 (1991).
[64] P. A. Zyla *et al.* (Particle Data Group Collaboration), Review of particle physics, Prog. Theor. Exp. Phys. **2020**, 083C01 (2020).
[65] J. W. F. Valle, Neutrino physics overview, J. Phys. Conf. Ser. **53**, 473 (2006).
[66] S. Bhattacharya, N. Sahoo, and N. Sahu, Singlet-doublet fermionic dark matter, neutrino mass and collider signatures, Phys. Rev. D **96**, 035010 (2017).
[67] T. Robens and T. Stefaniak, Status of the Higgs singlet extension of the standard model after LHC run 1, Eur. Phys. J. C **75**, 104 (2015).
[68] G. Chalons, D. Lopez-Val, T. Robens, and T. Stefaniak, The Higgs singlet extension at LHC run 2, Proc. Sci. ICHEP2016 (**2016**) 1180 [arXiv:1611.03007].
[69] S. Adhikari, I. M. Lewis, and M. Sullivan, Beyond the Standard Model effective field theory: The singlet extended Standard Model, Phys. Rev. D **103**, 075027 (2021).
[70] D. López-Val and T. Robens, Δr and the W-boson mass in the singlet extension of the standard model, Phys. Rev. D **90**, 114018 (2014).
[71] A. G. Akeroyd, M. Aoki, and H. Sugiyama, Lepton flavour violating decays $\tau \to \bar{l}ll$ and $\mu \to e\gamma$ in the Higgs triplet model, Phys. Rev. D **79**, 113010 (2009).
[72] U. Bellgardt *et al.* (SINDRUM Collaboration), Search for the decay $\mu^+ \to e^+e^+e^-$, Nucl. Phys. **B299**, 1 (1988).
[73] A. M. Baldini *et al.* (MEG Collaboration), Search for the lepton flavour violating decay $\mu^+ \to \mathrm{e}^+\gamma$ with the full dataset of the MEG experiment, Eur. Phys. J. C **76**, 434 (2016).
[74] M. Dutta, S. Bhattacharya, P. Ghosh, and N. Sahu, Singlet-doublet Majorana dark matter and neutrino mass in a minimal type-I seesaw scenario, J. Cosmol. Astropart. Phys. 03 (2021) 008.
[75] K. Griest and D. Seckel, Three exceptions in the calculation of relic abundances, Phys. Rev. D **43**, 3191 (1991).
[76] A. Chatterjee and N. Sahu, Resurrecting L-type sneutrino dark matter in light of neutrino masses and LUX data, Phys. Rev. D **90**, 095021 (2014).
[77] S. Patra, N. Sahoo, and N. Sahu, Dipolar dark matter in light of the 3.5 keV x-ray line, neutrino mass, and LUX data, Phys. Rev. D **91**, 115013 (2015).
[78] G. Belanger, F. Boudjema, A. Pukhov, and A. Semenov, Dark matter direct detection rate in a generic model with micromegas 2.2, Comput. Phys. Commun. **180**, 747 (2009).
[79] A. Semenov, LanHEP—A package for automatic generation of Feynman rules from the Lagrangian. Version 3.2, Comput. Phys. Commun. **201**, 167 (2016).
[80] J. M. Alarcon, L. S. Geng, J. Martin Camalich, and J. A. Oller, The strangeness content of the nucleon from effective field theory and phenomenology, Phys. Lett. B **730**, 342 (2014).
[81] M. Carena, A. Daleo, B. A. Dobrescu, and T. M. P. Tait, Z' gauge bosons at the Tevatron, Phys. Rev. D **70**, 093009 (2004).
[82] G. Cacciapaglia, C. Csaki, G. Marandella, and A. Strumia, The minimal Set of electroweak precision parameters, Phys. Rev. D **74**, 033011 (2006).

[83] G. Aad *et al.* (ATLAS Collaboration), Search for high-mass dilepton resonances using 139 fb^{-1} of pp collision data collected at $\sqrt{s} = 13$ TeV with the ATLAS detector, Phys. Lett. B **796**, 68 (2019).

[84] A. M. Sirunyan *et al.* (CMS Collaboration), Search for resonant and nonresonant new phenomena in high-mass dilepton final states at $\sqrt{s} = 13$ TeV, J. High Energy Phys. 07 (2021) 208.

[85] A. Das, P. S. B. Dev, Y. Hosotani, and S. Mandal, Probing the minimal $U(1)_X$ model at future electron-positron colliders via the fermion pair-production channel, arXiv:2104.10902.

[86] M. Aaboud *et al.* (ATLAS Collaboration), Search for new high-mass phenomena in the dilepton final state using 36.1 fb^{1} of proton-proton collision data at $\sqrt{s} = 13$ TeV with the ATLAS detector, J. High Energy Phys. 10 (2017) 182.

[87] G. Aad *et al.* (ATLAS Collaboration), Search for doubly and singly charged Higgs bosons decaying into vector bosons in multi-lepton final states with the ATLAS detector using proton-proton collisions at $\sqrt{s} = 13$ TeV, J. High Energy Phys. 06 (2021) 146.

[88] P. Pal, *An Introductory Course of Particle Physics* (CRC Press, Taylor & Francis Group, Boca Raton, FL, 2014).